Astronomy & Astrophysics manuscript no. paperinglese
October 9, 2009

New identified (^{3}H)4d-(^{3}H)4f transitions of Fe II from UVES spectra of HR 6000 and 46 Aql⋆, ⋆⋆

F. Castelli[1], R.L. Kurucz[2], and S. Hubrig[3]

[1] Istituto Nazionale di Astrofisica– Osservatorio Astronomico di Trieste, Via Tiepolo 11, I-34131 Trieste, Italy
e-mail: castelli@oats.inaf.it
[2] Harvard-Smithsonian Center for Astrophysics, 60 Garden Street, Cambridge, MA 02138, USA
[3] Astrophysical Institute Potsdam, An der Sternwarte 16, D-14482 Potsdam, Germany

ABSTRACT

Aims. The analysis of the high-resolution UVES spectra of the CP stars HR 6000 and 46 Aql has revealed the presence of an impressive number of unidentified lines, in particular in the 5000-5400 Å region. Because numerous 4d-4f transitions of Fe II lie in this spectral range, and because both stars are iron overabundant, we investigate whether the unidentified lines are Fe II.
Methods. ATLAS12 model atmospheres with parameters $T_{\rm eff}$=13 450 K, log g=4.3 and $T_{\rm eff}$=12 560 K, log g=3.8 were computed for the individual abundances of the stars HR 6000 and 46 Aql, respectively, to use them as spectroscopic sources to identify Fe II lines and determine Fe II gf-values. After identifying several unknown lines in the stellar spectra as (^{3}H)4d–(^{3}H)4f transitions of Fe II, we derived astrophysical log gf-values for them. The energies of the upper levels were assigned on the basis of both laboratory iron spectra and predicted energy levels.
Results. We determined 21 new levels of Fe II with energies between 122 910.9 cm^{-1} and 123 441.1 cm^{-1}. They allowed us to add 1700 new lines to the Fe II linelist in the wavelength range 810 − 15011 Å. Many of these lines are sufficiently strong to contribute to the spectra of Population I late B-type stars, even when their iron abundance is subsolar. In the 5000-6000 Å region discussed in this paper, the astrophysical and computed log gf-values show good general agreement and greatly improve the synthetic spectrum of both HR 6000 and 46 Aql. However many features remain unidentified indicating that further work to classify Fe II high energy levels has still to be done

Key words. line:identification-atomic data-stars:atmospheres-stars:chemically peculiar- stars:individual:HR 6000 and 46 Aql

1. Introduction

The analysis of the UVES spectrum of the chemically peculiar star HR 6000 performed by Castelli & Hubrig (2007) identified a large number of unidentified lines across the entire observed range from 3050 Å to 9460 Å. Regions in which the most impressive results were obtained are those at 4404-4411 Å and 5000-5400 Å. An attempt to identify unknown lines in the 5130-5136 Å interval using the available lists of predicted Fe II lines [1] (version 2003) was laborious and unsuccessful.

An analysis of both the list of unidentified lines and of the plot of the observed and computed spectra available at the Castelli web-site[2] led S. Johansson to identify about half of them as transitions between high excitation levels of Fe II. These identifications were made using unpublished line lists that he had obtained from laboratory spectra. Johansson (2009) was able to identify a group of 13 lines concentrated in the 4404-4411 Å interval as belonging to the multiplet 4s(^{7}S)4d ^{8}D – 4s(^{7}S)4f ^{8}F. The upper terms have energies of between 132 145 cm^{-1} and 132 158 cm^{-1}, and are therefore well above the Fe II ionization limit of 130 563 cm^{-1}. Another example of new identifications can be found in Castelli, Johansson & Hubrig (2008), where some unknown lines in the 5175-5180 Å interval of HR 6000 were identified with (^{3}H)4d – (^{3}H)4f transitions of Fe II. In this case, the energy of the upper levels is of the order of 123 000 cm^{-1}, and therefore just below the ionization limit.

Laboratory spectroscopic sources produce emission lines and must populate upper energy levels to produce such a spectrum. Most stars have spectra with lines in absorption, so that the line strength is determined from the lower energy level populations; for this reason, stellar lines are stronger than laboratory lines. HR 6000 and 46 Aql are bright and can be observed at high resolution and high signal-to-noise ratio. They have low projected rotation velocity, 1.5 km s^{-1} for HR 6000, and 1.0 km s^{-1} for 46 Aql. Thus, blending is minimal and wave-

Send offprint requests to: F. Castelli

⋆ This study is the result of a collaboration with S. Johansson, who unfortunately died before this paper started to be written

⋆⋆ Tables 4, 5, 6, and the Appendices A and B are only available in electronic form at http://www.aanda.org

[1] http://kurucz.harvard.edu/atoms/2601/gf2601.lines0600
[2] http://wwwuser.oat.ts.astro.it/castelli/hr6000/hr6000.html

lengths and line strengths can be determined well by fitting the spectrum.

It is likely that most of the unidentified lines in these stars are those of Fe II. Some could be due to other overabundant elements, in particular P II, Mn II, and Xe II. However, as far as Mn II is concerned, the unidentified lines are either weaker or do not appear at all in the HgMn star HD 175640, which is iron weak ([Fe/H]= −0.25) and manganese overabundant ([Mn/H]= +2.4) (Castelli & Hubrig 2004; Castelli et al. 2008). It is also improbable that such a large number of unidentified lines, mostly concentrated in the 5000-6000 Å region, are not also due to Fe II. Since these lines are present at subsolar iron abundances, they must be present in all Population I late B-type stars, or in any object with strong Fe II lines, but they are normally smeared out by rotation and difficult to see.

Because every new energy level accounts for hundreds of new lines throughout the spectrum from the UV through to the IR wavelength regions, we extended to a wider range previous work for the 5175-5181 Å interval with the aim of increasing the number of the classified Fe II levels. We used identifications both based on laboratory spectra and derived from predicted energy levels. Furthermore, because numerous high-excitation lines from the $3d^6(^5D)4d - 3d^6(^5D)4f$ transitions are observed in the 5000−5400 Å interval, we examined the computed log gf-values used in the synthetic spectra computations. We compared them with both experimental (Johansson, 2002) and astrophysical values, which we derived from the lines of both HR 6000 and 46 Aql. We used two stars to check the consistency and estimate the reliability of the astrophysical oscillator strengths. We then derived astrophysical log gf-values for the new identified (^{3}H)4d − (^{3}H)4f lines. Finally, we show an example of synthetic spectrum computed both with old and new line lists.

To use HR 6000 and 46 Aql as spectroscopic sources for identifying Fe II lines, to determine Fe II log gf-values, and to compute synthetic spectra, we fixed at first the model atmosphere and the abundances for each star. Special care was devoted to deriving the iron abundance.

2. The stars HR 6000 and 46 Aql

Both HR 6000 (HD 144667) and 46 Aql (HD 186122) are B-type CP stars. HR 6000 was extensively studied by Castelli & Hubrig (2007) in the 3050 − 9460 Å region, and 46 Aql, by Sadakane et al. (2001) in the 5100 − 6400 Å interval. Because model atmospheres are needed to determine astrophysical log gf-values, we revised the model atmosphere and the abundances of HR 6000 and determined the model atmosphere and the abundances for 46 Aql on the basis of our observations.

2.1. Observations

The observations of HR 6000 are described in Castelli & Hubrig (2007). Those for 46 Aql were obtained in the framework of the same observational program (ESO prg. 076.D-0169(A)). They are of the same quality and were reduced with the same procedures used for HR 6000.

For this paper, we revised our previous analysis of HR 6000 (Castelli & Hubrig 2007) because further investigation indicated that the Balmer profiles used by us to derive the model parameters are too affected in the UVES spectra by imperfections related to the echelle orders. As we show in Appendix A, the spectral distortions for H_δ, H_γ, and, to a less extent, for H_β are so significant that it is impossible to determine a reliable continuum level for the observed profiles. Only H_α does not appear to be affected by these problems, so it could be used for the analysis with some confidence.

2.2. Model parameters and abundances

In Castelli & Hubrig (2007), the model parameters of HR 6000 ($T_{\rm eff}$=12850 K, log g=4.10, ξ=0.0 km s^{-1}) were derived from both Balmer profiles and Fe I and Fe II ionization equilibrium. In this paper, the model parameters for both HR 6000 and 46 Aql were obtained from the Strömgren photometry, from the requirement that there was no correlation between the Fe II abundances derived from high and low excitation lines, and from the constraint of Fe I − Fe II ionization equilibrium. This type of determination led to a revision of the model parameters for HR 6000.

The parameters of the two stars obtained from the Strömgren photometry are given in Table 1. They were derived with the method described in Castelli & Hubrig (2007), where the reddening for HR 6000 is also discussed. The observed indices were taken from the Hauck& Mermilliod (1998) catalogue[3]. ATLAS9 models with parameters [13 800K, 4.3] for HR 6000 and [12 750K, 3.8] for 46 Aql were computed for solar abundances and zero microturbulent velocity. The iron abundance was derived from the equivalent widths of a selected sample of high-excitation Fe II lines with experimental log gf-values available from Johansson (2002). They are due to (^{5}D)4d − (^{5}D)4f transitions and are listed in Table 2. The equivalent widths of these lines, as well as of the other lines discussed in this paper, were measured by integrating the residual fluxes over the profiles. Abundances were obtained with a Linux version (Castelli 2005) of the WIDTH code (Kurucz 1993). We note that there are no measured equivalent widths for the line at 5100.734 Å because it is part of a strong blend formed by four Fe II lines. The line was included in Table 2 to show the whole set of (^{5}D)4d − (^{5}D)4f transitions for which experimental log gf-values are available. The lines from Table 2 are particularly well suited to providing the iron abundance because they are rather insensitive to the model parameters. In fact, for differences in $T_{\rm eff}$ of 500 K, the abundance difference is less than 0.05 dex; for differences in log g of 0.2 dex, the abundance difference is of the order of 0.01 dex. For example, for HR 6000, the Fe II abundance from ATLAS9 models computed for log g=4.3, and $T_{\rm eff}$= 13 300 K, 13 800 K, and 14 300 K, is −3.66 dex , −3.65 dex (Table 2), and −3.61 dex, respectively. For models computed for $T_{\rm eff}$=13 800 K, and log g=4.1, 4.3, and 4.5, the iron abundance is −3.65 dex, −3.65 dex (Table 2), and −3.64 dex. Similar results were obtained for 46 Aql.

[3] http://obswww.unige.ch/gcpd/gcpd.html

Table 1. Observed and dereddened Strömgren indices for HR 6000 and 46 Aql.

Star	b−y	m	c	β	E(b-y)	(b-y)$_0$	m$_0$	c$_0$	$T_{\rm eff}$(K)	log g
HR 6000	−0.030	0.116	0.521	2.750	0.031	−0.061	0.126	0.506	13799±150	4.27±0.05
	±0.003	±0.003	±0.003							
46 Aql	−0.019	0.094	0.641	2.729	0.035	−0.054	0.105	0.634	12763±150	3.75±0.05
	±0.002	±0.002	±0.002							

Table 2. Iron abundance derived from a selected sample of high excitation (4d-4f) Fe II lines with experimental log gf-values and ATLAS9 models.

λ(Å)	log gf	χ_{low}(cm^{-1})	χ_{up}(cm^{-1})	Config.	W(mÅ)	logϵ(W)	W(mÅ)	logϵ(W)
	exp				HR 6000 [13 800,4.3]		46 Aql [12 750,3.8]	
4883.292	−0.521	82 853.66	103 325.93	(^{5}D)4d e^{6}F$_{11/2}$− (^{5}D)4f 3[5]$_{11/2}$	14.2	−3.87	11.3	−4.10
4913.295	0.016	82 978.67	103 325.93	(^{5}D)4d e^{6}F$_{9/2}$− (^{5}D)4f 3[5]$_{11/2}$	36.3	−3.67	31.1	−3.91
5001.953	0.933	82 853.66	102 840.27	(^{5}D)4d e^{6}F$_{11/2}$− (^{5}D)4f 4[6]$_{13/2}$	76.0	−3.61	66.1	−3.86
5100.734	0.671	83 726.37	103 325.93	(^{5}D)4d ^{6}D$_{9/2}$− (^{5}D)4f 3[5]$_{11/2}$	−−	−−	−−	−−
5227.483	0.831	84 296.83	103 421.16	(^{5}D)4d e^{6}G$_{11/2}$− (^{5}D)4f 3[6]$_{13/2}$	66.8	−3.58	58.0	−3.83
5253.647	−0.191	84 296.83	103 325.93	(^{5}D)4d e^{6}G$_{11/2}$− (^{5}D)4f 3[5]$_{11/2}$	30.6	−3.51	23.5	−3.83
5260.254	1.090	84 035.12	103 040.32	(^{5}D)4d e^{6}G$_{13/2}$− (^{5}D)4f 4[7]$_{15/2}$	77.9	−3.59	66.9	−3.84
5316.214	0.418	84 035.12	102 840.27	(^{5}D)4d e^{6}G$_{13/2}$− (^{5}D)4f 4[6]$_{13/2}$	48.7	−3.61	39.7	−3.94
5339.592	0.568	84 296.83	103 019.64	(^{5}D)4d e^{6}G$_{11/2}$− (^{5}D)4f 4[7]$_{13/2}$	48.2	−3.74	42.8	−3.97
5387.063	0.593	84 863.33	103 421.16	(^{5}D)4d e^{4}G$_{11/2}$− (^{5}D)4f 3[6]$_{13/2}$	47.7	−3.75	41.3	−4.00
5414.852	−0.258	84 863.33	103 325.93	(^{5}D)4d e^{4}G$_{11/2}$− (^{5}D)4f 3[5]$_{11/2}$	25.0	−3.57	19.1	−3.87
5506.199	0.923	84 863.33	103 019.64	(^{5}D)4d e^{4}G$_{11/2}$− (^{5}D)4f 4[7]$_{13/2}$	73.8	−3.65	54.2	−3.94
5510.783	0.043	85 184.73	103 325.93	(^{5}D)4d e^{4}G$_{9/2}$− (^{5}D)4f 3[5]$_{11/2}$	32.5	−3.61	26.3	−3.89
Average abundances						−3.65±0.09		−3.92±0.08

After having determined the iron abundance, we checked the model parameters by inquiring whether the adopted model gives the same abundance for Fe I lines and for a large sample of Fe II lines including low-excitation transitions. To this purpose, we measured the equivalent widths of the Fe I and Fe II lines listed in Table B.1 and derived the corresponding abundances. They are −3.68±0.06 dex and −3.68±0.15 dex, respectively, for HR 6000 and −3.93±0.06 dex and −3.91±0.11 dex, respectively, for 46 Aql. For both stars, the ionization equilibrium condition is fulfilled within the error limits, and the Fe II abundance derived from the large sample of lines listed in Appendix B agrees, within the error limits, with the abundance yielded by the small sampl of high-excitation Fe II lines listed in Table 2. We conclude that the [13 800,4.3] ATLAS9 model for HR 6000 and the [12 750K,3.8] ATLAS9 model for 46 Aql not only reproduce the respective Strömgren colors, but also satisfy the constraints of both the Fe I-Fe II ionization equilibria and Fe II abundance, independent of the excitation potential. The H$_\alpha$ profile is also fairly well reproduced by the models in both stars.

The ATLAS9 models were used to obtain abundances for elements other than iron. For He I, we adopted the lines listed in Castelli & Hubrig (2004) and analyzed them as described in that paper. For the other elements, the lines listed in Table B.1 were used. For most lines, equivalent widths were measured. For weak lines or lines that are blends of transitions belonging to the same multiplet, such as Mg II 4481 Å, and most O I profiles, we derived the abundance from the line profiles with the synthetic spectrum method. Synthetic spectra were computed with a Linux version (Sbordone et al. 2004) of the SYNTHE code (Kurucz 2005). When no lines were observed for a given element an upper abundance limit was determined by reducing the intensity of the computed line at the noise level. To compute synthetic spectra, rotational velocities equal to 1.5 km s^{-1} and 1.0 km s^{-1} were adopted for HR 6000 and 46 Aql, respectively. They were derived by comparing the observed and computed Mg II profiles at 4481 Å.

Because the abundances found for most elements were far from solar, we computed ATLAS12 models (Kurucz 2005) for the individual abundances with the same parameters as determined for the ATLAS9 models. The structure of the ATLAS12 models is heavily affected by the large iron overabundance, while the helium underabundance, although large, has a negligible effect, in contrast to what was wrongly stated in Castelli & Hubrig (2007). As a consequence, the Fe I–Fe II ionization equilibrium is no longer achieved by the ATLAS12 models unless the parameters are changed. Because the gravity affects the wings of the Balmer profile more than the temperature does, we kept fixed the gravity which reproduces the H$_\alpha$ profile rather well and modified $T_{\rm eff}$ until the Fe I abundance from the lines listed in Appendix B agrees with the Fe II abundance obtained from the lines shown in Table 2. The final ATLAS12 parameters are $T_{\rm eff}$=13 450 K, log g=4.3, and ξ=0.0 km s^{-1} for HR 6000 and $T_{\rm eff}$=12 560, log g=3.8, and ξ=0.0 km s^{-1} for 46 Aql. The computed indices (b-y), m, and c for HR 6000 are −0.064, 0.126, and 0.535, respectively. For 46 Aql, they are

−0.052, 0.116, and 0.662. For both stars, the observed (b-y) is reproduced by the models within the observational uncertainties, while the c index is not. This means that the models are able to predict the optical spectrum but not the spectrum shortward of the Balmer discontinuity.

We note that we could simply have used the ATLAS9 models computed for solar abundances with the parameters given in Table 2, which reproduce both the Strömgren colors and the criteria for Fe I-Fe II ionization equilibrium. However in this case, the number densities of the input model are different from those computed by the final synthetic spectrum on the basis of non solar abundances for several elements, in particular for helium which heavily affects the state equation results. We preferred to use consistent computations in model and synthetic spectra rather than use different sets of abundances in the two cases, even though predictions more close to obsevations may be achievable when different abundances are indeed used for model atmosphere and synthetic spectrum.

Table 3 summarizes the final stellar abundances used to compute ATLAS12 models and synthetic spectra. For HR 6000, abundances that differ from previous determinations (Castelli & Hubrig 2007) by 0.2 dex or more are those for He I (+0.20), Ca II (+0.2), Ti II (+0.30), Cr II (+0.27), Mn II (+0.42), Fe I and Fe II (+0.21), and Y II (+0.2). For 46 Aql, abundances differing by more than 0.2 dex from those derived by Sadakane et al. (2001) are those for C II (−0.33), S II (≥+0.77), Ti II (−0.44), and Fe I (−0.32). The number in parenthesis is the difference between the abundance determined in this paper and that from the other analyses. Sadakane et al. (2001) adopted an ATLAS9 model atmosphere with parameters $T_{\rm eff}$=13 000K, log g=3.65, and v_{turb}=0.3 km s^{-1}.

The abundances of 46 Aql have approximately the same pattern as in HR 6000, but the deviations from solar values are generally lower. The most remarkable differences between the two stars are the overabundance of copper, zinc, and arsenic in 46 Aql, while no lines of these elements were observed in HR 6000. The arsenic overabundance cannot be quantified owing to the lack of log gf data for As II. Lines of As II observed in the spectrum are listed in Table B.1. To each line, we assigned the corresponding transition on the basis of the two separate lists of lines and energy levels taken from the NIST database[4,5]. Furthermore, Cr II is slightly overabundant in HR 6000 ([0.3]) and underabundant in 46 Aql [−1.1], Ca II is solar in HR 6000 and slightly underabundant in 46 Aql [−0.3], and Y II and Hg II are less overabundant in HR 6000 than in 46 Aql.

In both HR 6000 and 46 Aql, the He I profiles cannot be reproduced by the same abundance. We adopted the abundance that reproduced the wings of the lines at $\lambda\lambda$ 3867, 4026, and 4471 Å the most closely.. The cores of all He I lines would require a lower abundance than that reproducing the wings.

In both stars, the average abundances of phosphorous and manganese have deviations larger than 0.2 dex. For phosphorous, these are caused by a difference of the order of 0.5 dex between the abundance from lines with $\lambda < 5\,000$ Å and the abundance from lines with $\lambda > 5\,000$ Å. For manganese, the large deviation is due to a difference of 0.6 dex in HR 6000 and 0.4 dex in 46 Aql between the abundances from lines lying shortward and longward of the Balmer discontinuity. The Mn II abundance was derived from both equivalent widths and line profiles. In the first case, no hyperfine structure was considered in the computations, while in the second case hyperfine components were taken into account for all the lines except for 3917.318 Å, for which no hyperfine constants are available for its upper energy level. The hyperfine components were taken from Kurucz[6]. The differences between the average abundances obtained by the two methods are of the order of 0.01 dex.

A plausible explanation of the discrepancy in the Mn II abundance is that the model structure is inadequate to reproduce the ultraviolet spectrum, as already deduced by comparing the computed and observed c indices. Vertical abundance stratification, which is a consequence of radiative diffusion acting in CP stars (Michaud 1970), can be invoked to explain the anomalous He I line profiles as well as the phosphorus and manganese inhomogeneous abundances. A comprehensive discussion of observational evidence for the abundance stratification in CP stars is given by Ryabchikova et al. (2003). It describes both the impossibility of fitting the wings and the core of strong spectral lines with the same abundance, and the differences in the abundances measured from the lines of the same ion that form at different optical depths, as, for instance, in the case of lines both longward and shortward of the Balmer discontinuity. Finally, for a reliable discussion on phosphorus, more oscillator strengths data of P II and P III lines observed in the optical region are needed.

In both HR 6000 and 46 Aql, the Hg II line at 3983.890 Å is due mostly to the heaviest isotope of Hg. The lines of the Ca II infrared triplet at 8498, 8542, and 8662 Å are red-shifted by 0.14 Å in HR 6000 and by 0.13 Å in 46 Aql, so indicating a non solar Ca isotopic composition. In HR 6000, emission lines of Cr II, Mn II, and Fe II were observed. In the spectrum of 46 Aql, instead, there are emission lines of Ti II and Mn II.

3. The (^{5}D)4f and (^{3}H)4f states of Fe II

Energy levels of a given atom are described most often by the LS coupling in which the total orbital angular momentum **L** of the atom is coupled with the total spin angular momentum **S** to produce the total angular momentum **J=L+S**. Some high levels, such as the (^{5}D)4f and (^{3}H)4f states of Fe II, tend to appear in pairs, so they are more accurately described by the jK coupling with the notation $j_c[K]_J$, where $\mathbf{j}_c$ is the total angular momentum of the core and $\mathbf{K}=\mathbf{j}_c+\mathbf{l}$ is the coupling of $\mathbf{j}_c$ with the orbital angular momentum **l** of the active electron. The level pairs correspond to the two separate values of the total angular momentum **J** obtained when the spin **s**=±1/2 of the active electron is added to **K**.

While the energy levels of the 3d^6(^{5}D)4f states are known and available for instance in the NIST database, this is not the case for the levels with the higher parent term 3d^6(^{3}H)4f. Most

[4] http://physics.nist.gov/PhysRefData/ADS/lines_form.html
[5] http://physics.nist.gov/PhysRefData/ADS/levels_form.html
[6] http://kurucz.harvard.edu/atoms/2501/hyper250155.srt

Table 3. Abundances log(N(elem)/N_{tot}) for HR 6000 and 46 Aql from ATLAS12 models. Solar abundances are from Grevesse & Sauval (1998).

elem	HR 6000 [13450K,4.3]	46 Aql [12560K,3.8]	Sun
He I	−2.10	−2.00	−1.05
Be II	−9.78	−9.91	−10.64
C II	−5.50	−4.75	−3.52
N I	≤−5.82	≤−5.50	−4.12
O I	−3.68±0.4	−3.51±0.10	−3.21
Ne I	≤−4.86	−4.51	−3.96
Na I	≤ −5.71	−5.69	−5.71
Mg II	−5.66	−5.45	−4.46
Al I	≤−7.30	−6.65	−5.57
Al II	≤−7.30	≤ −7.40	−5.57
Si II	−7.35	−5.61±0.06	−4.49
P II	−4.44±0.27	−5.02±0.30	−6.59
P III	−5.11±0.26	−5.87	−6.59
S II	−6.26	−5.74	−4.71
Cl I	≤−7.74	≤−7.04	−6.54
Ca II	−5.68	−5.98	−5.68
Sc II	≤ −9.50	≤−9.50	−8.87
Ti II	−6.47±0.13	−6.46±0.06	−7.02
V II	≤ −9.14	−8.94	−8.04
Cr II	−6.10±0.09	−7.48	−6.37
Mn II	−5.18±0.32	−5.82±0.22	−6.65
Fe I	−3.65±0.07	−3.91±0.06	−4.54
Fe II	−3.65±0.09	−3.91±0.08	−4.54
Co II	≤−8.42	≤ −8.02	−7.12
Ni II	−6.24	−6.47	−5.79
Cu II	≤−7.83	−6.24±0.02	−7.83
Zn I	−−	−5.85	−7.44
Zn II	−−	−5.76	−7.44
As II	−−	>−9.67	−9.67
Sr II	≤−10.07	−10.67	−9.07
Y II	−8.60	−8.09±0.08	−9.80
Xe II	−5.23	−5.81	−9.87
Hg II	−8.20	−7.10	−10.91

of these levels have not been observed in the laboratory and remain unclassified.

4. The $3d^6(^5D)4d - 3d^6(^5D)4f$ transitions of Fe II

The 4d-4f transitions discussed in this paper appear in the optical region, mostly between 4800 and 6000 Å. Their presence in stellar spectra was found a long time ago by Johansson & Cowley (1984). They are also present in the spectra of the iron-rich peculiar stars HR 6000 and 46 Aql. We used UVES spectra of these stars to derive values of astrophysical log gf that we compared with experimental and computed values.

4.1. *Experimental* log gf*-values*

All the experimental data described in this section were made available to F. Castelli by S. Johansson and are briefly described in Johansson (2002). Radiative lifetime measurements of five $3d^6(^5D)4f$ levels, i.e., $4[6]_{13/2}$, $4[7]_{13/2}$, $4[7]_{15/2}$, $3[6]_{13/2}$, $3[5]_{11/2}$, and branching fraction measurements for 13 transitions 4d-4f with wavelengths in the 4800-5800 Å region were performed at Lund. Einstein coefficients A, derived by combining the measured branching fractions with the lifetime measurements, were converted into experimental oscillator strengths. The 4d−4f transitions together with the experimental log gf-values are given in Tables 2 and 4. While the 4f levels with J >11/2 decay only to 4d levels, the 4f $3[5]_{11/2}$ level may decay to 3d levels as well. As a consequence, the log gf-value for the transitions involving the $3[5]_{11/2}$ level may be less accurate than those related to levels with J>11/2, which have an estimated error of 0.05 dex.

4.2. *Computed* log gf*-values*

The computed log gf-values were taken from both Kurucz's line lists (K09, January, 2009 version)[7] and Raassen & Uylings (1998) (RU98) data. We note that Fuhr & Wiese (2006) (FW06) adopted the RU98 data for the few (^{5}D)4d − (^{5}D)4f transitions that they listed in their critical compilation.

Both K09 and RU98 results were obtained with semi-empirical methods, although different ones. The K09 results were obtained with the use of the Cowan (1981) atomic structure code, while the RU98 results were obtained by the orthogonal operators method. The computed log gf-values are listed in Table 4.

4.3. *Astrophysical* log gf*-values*

To derive astrophysical log gf-values we computed synthetic profiles for the Fe II lines listed in Table 4. We used the ATLAS12 models discussed in Sect. 2, the SYNTHE code (Kurucz 2005), and line lists based on the Kurucz database that we continually update with new data when available (Castelli & Hubrig 2004). By fixing the iron abundance to −3.65 dex for HR 6000 and to −3.91 dex for 46 Aql (Table 3), we adjusted the log gf- values in the calculated spectrum, for the lines listed in Table 4, until observed and computed profiles were in optimal agreement. All the lines can be fitted well except for the very strong ones with log gf higher than 0.9. Their observed cores are stronger than those computed and can never be reproduced by the computed spectrum because increasing the log gf-value broadens the wings instead of increasing the core. An example is the line at 5260.254 Å, which we decided to exclude from our comparisons. The strongest Fe II lines are possibly affected by iron abundance vertical stratification, which does not affect the medium-strong and weak lines.

Figure 1 shows the difference between the astrophysical log gf-values from both HR 6000 and 46 Aql as function of the astrophysical log gf of HR 6000. The average difference, shown by the dashed line, is −0.019±0.042 dex, but for single lines the difference increases with increasing log gf from 0.00 to 0.15 dex, in the sense that the values from 46 Aql become larger than those from HR 6000. The largest difference of −0.15 dex occurs for λ 5961.705 Å. Because each astrophysi-

[7] http://kurucz/harvard/edu/atoms/2601/gf2601kjan09.pos

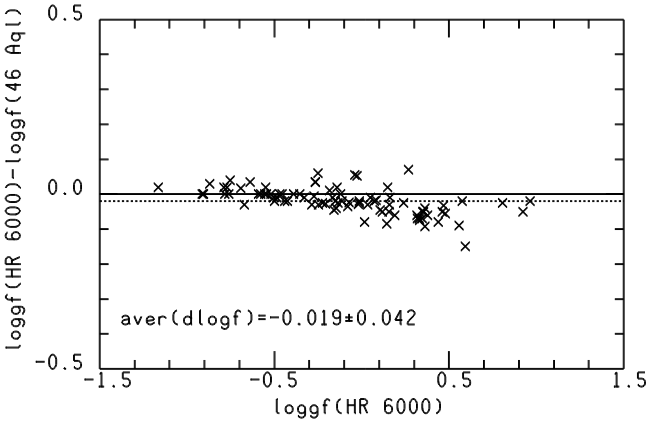

Fig. 1. Comparison of astrophysical log gf-values from HR 6000 and 46 Aql for (^{5}D)4d-(^{5}D)4f transitions of Fe II. The horizontal dashed line indicates the average difference.

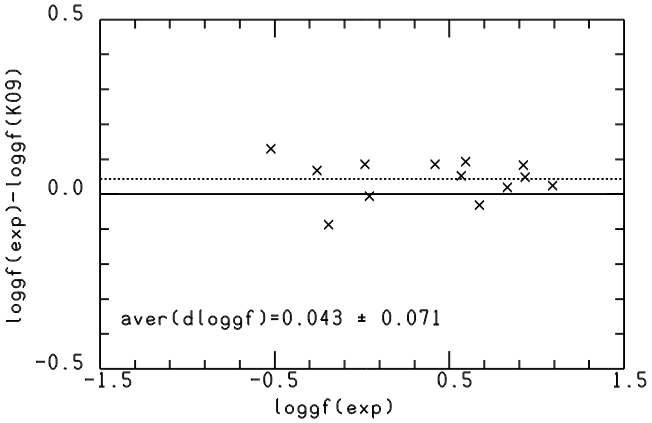

Fig. 2. Calculated log gf-values (K09) for (^{5}D)4d-(^{5}D)4f transitions of Fe II are compared with experimental log gf-values. The horizontal dashed line indicates the average difference.

cal value reproduces the observed line in each star well we do not have an explanation of this discrepancy.

As astrophysical log gf-values we assumed the average of the values obtained from HR 6000 and 46 Aql. Astrophysical log gf-values for both the two stars and the average are listed in Table 4.

4.4. Comparison of values of log gf

The difference between experimental and computed log gf-values versus the experimental log gf is shown Figs. 2 and 3, where the computed data are those from K09 and RU98, respectively. The average difference of 0.028±0.061 dex yielded by the RU98 values is lower than the average difference of 0.043±0.071 dex given by the K09 values, but they agree within the error limits. The largest difference of +0.130 in Fig. 2 is due to the transition at 4883.292 Å. However, the J value of the 4f upper level of this line is 11/2, which is not high enough to ensure that there are no additional decays to 3d levels (Johansson, 2002). This fact could affect the experimental log gf-value and the closer agreement with the RU98 data may be fortuitous. In fact, Table 4 shows that the astrophysical log gf-value agrees more closely with the K09 than the RU98 value.

Astrophysical log gf-values are compared with log gf-values from K09 and RU98 in Figs. 4 and 5, respectively. The mean difference of 0.006±0.116 dex given by the K09 data is fully comparable with the average difference of −0.007±0.144 dex yielded by the RU98 log gf-values. In both cases, the dispersion around the mean value is rather large. The lines giving the largest discrepancies are different for K09 and RU98. In K09, the lines are those at wavelengths of $\lambda\lambda$ 5257.119 (−0.47), 5359.237 (−0.314), 5358.872 (+0.286), 5355.421 (+0.285), 5366.210 (−0.267), 5062.927 (−0.260) Å. In RU98 they are those with wavelength $\lambda\lambda$ 5070.583 (−0.760), 5140.689 (−0.543), 5093.783 (−0.399), 5200.798 (+0.287), 5081.898 (−0.279) Å. The values in parentheses are the difference log gf(computed) − log gf(astrophysical). For all of these transitions, the difference between the astrophysical

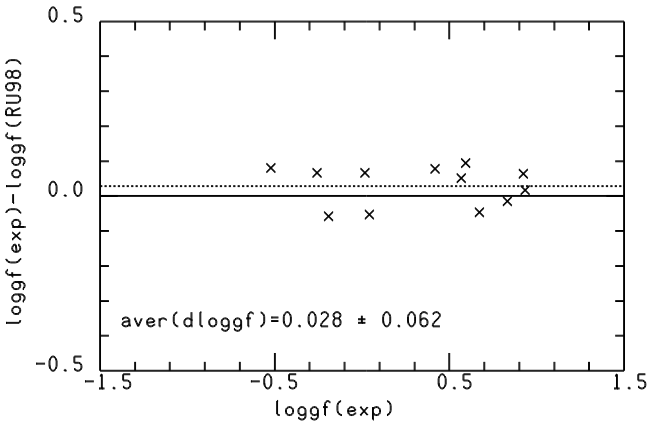

Fig. 3. Calculated log gf-values (RU98) for (^{5}D)4d-(^{5}D)4f transitions of Fe II are compared with experimental loggf-values. The horizontal dashed line indicates the average difference

log gf-values from HR 6000 and 46 Aql is less than 0.06 dex, so that the cause of the disagreements is probably due to the computed values.

We note that Kurucz updates his calculation whenever new Fe II levels become available. The January 2009 version of the Fe II linelist used for the (^{5}D)4d−(^{5}D)4f transitions discussed in this paper includes only a few of the new (^{3}H)4d−(^{3}H)4f levels presented in Sect.5. In the near future, a new Fe II linelist with all the new levels given in Tables 5 and 6 will be made available at the Kurucz web-site.

5. The new identifications in HR 6000 and 46 Aql

The spectrum of HR 6000 contains an enormous number of unidentified lines mostly concentrated in the 5000-5400 Å region (Castelli & Hubrig, 2007). The same unidentified lines can also be observed in the spectrum of 46 Aql. S. Johansson (2006) remarked that a great number of unidentified lines in the plots of HR 6000 available at the Castelli web-site (see footnote 2), are also present in laboratory iron spectra. He therefore

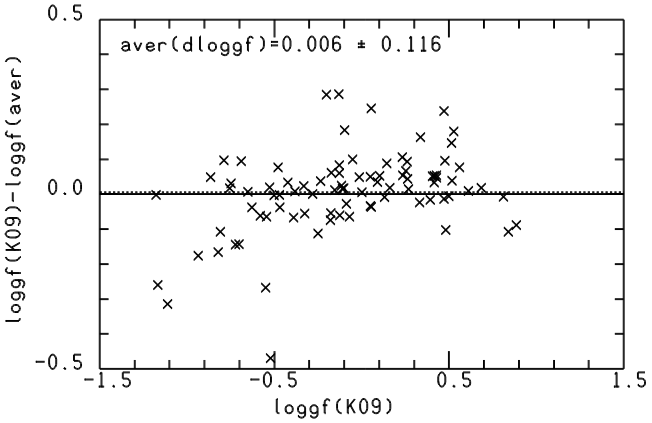

Fig. 4. Calculated log gf-values (K09) for (^{5}D)4d-(^{5}D)4f transitions of Fe II are compared with astrophysical log gf-values. The horizontal dashed line indicates the average difference.

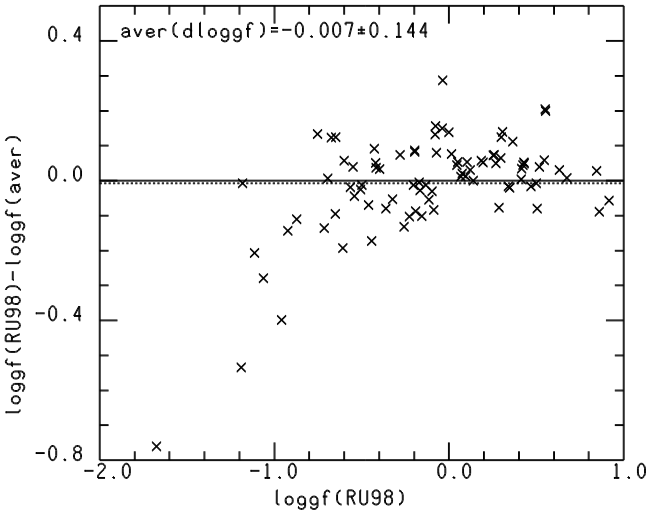

Fig. 5. Calculated log gf-values (RU98) for (^{5}D)4d-(^{5}D)4f transitions of Fe II are compared with astrophysical log gf-values. The horizontal dashed line indicates the average difference.

identified several unknown features in the 4000-5500 Å interval of HR 6000 as beign produced by iron. These identifications are at different levels of completeness. In a few cases, the transition is identified only as Fe , in most cases, as Fe II, and in some cases, as Fe II with both levels of the transition being classified.

5.1. The $3d^6(^3H)4d - 3d^6(^3H)4f$ transitions of Fe II

Most of the Fe II lines classified by S. Johansson are due to the (^{3}H)4d-(^{3}H)4f transitions. Their lower excitation potential is higher than 103 800 cm^{-1} (12.87 eV) and their upper excitation potential is of the order of 123 000 cm^{-1} (15.25 eV), and therefore close to the ionization limit of 130 563 cm^{-1} (16.19 eV).

In preliminary work, Castelli et al. (2008) provide an example in both HR 6000 and 46 Aql of four lines at 5176.711, 5177.3896, 5177.7762, and 5179.536 Å identified for the first time with Fe II (^{3}H)4d-(^{3}H)4f transitions. Only for two lines (at 5177.3896 and 5179.539 Å) were energies and terms known for both levels, while for the other two lines (at 5176.711 and 5179.536 Å) the term of the upper level was unknown, except for the J quantum number. Further lines and energies indicated by S. Johansson are those marked with a "J" in Table 5.

To complete and extend the number of the identifications, we proceeded as follows. We started from the "J" lines. Knowing the term, the energy of the lower level of a "J" line was determined using either the NIST database (see footnote 4) or the Kurucz linelists (see footnote 1). A given (^{3}H)4d-(^{3}H)4f transition was then searched for among the Fe II predicted lines available in the Kurucz database (version 2007). For this search, both the lower energy level and the J quantum number of the upper level were used as key parameters. Once the predicted line corresponding to the new identified transition was fixed, the predicted energy was replaced by the energy assigned by S. Johansson to the level. This substitution was made not only for the given line but also for all lines with that predicted level as their upper level. We then compared the pattern of the computed log gf-values with the pattern of astrophysical log gf-values for those lines. If they were similar, we accepted the identification. If not, we tried another match. In this way, because of the J lines, we fixed 11 new energy levels and all the transitions with a new level as an upper level. In addition, we determined another 10 new levels from predicted lines. For a given predicted upper level, we searched in the spectrum for unidentified lines with similar intensity and the same wavelength difference as the predicted lines. We selected the lines with positive log gf-values, or even negative, but close to zero. The observed wavelength and the known lower energy level were then used to fix the upper level of the transitions.

Table 5 lists both the (^{3}H)4d-(^{3}H)4f transitions originally identified by S. Johansson and those that we derived from the above described procedure. The letter "J" is associated with the first group of lines, the letter "K" with the second group. Not all the lines listed in Table 5 are observable in the spectra, so that values of astrophysical log gf cannot be assigned to all lines. The last column of Table 5 lists lines observed in HR 6000 that were listed as unidentified lines by Castelli & Hubrig (2007).

Figure 6 compares astrophysical log gf-values from HR 6000 and 46 Aql. It is the analogous to Fig. 1, but for the (^{3}H)4d-(^{3}H)4f transitions. The average difference, shown by the dashed line, is negligible, but the scatter is larger than that obtained for the (^{5}D)4d-(^{5}D)4f transitions. The reason is the very low intensity of some of the (^{3}H)4d-(^{3}H)4f transitions, which makes the fitting of the profile problematic. As for the (^{5}D)4d-(^{5}D)4f transitions, we assumed astrophysical log gf-values to be the average of values obtained for HR 6000 and 46 Aql, but we excluded the lines for which astrophysical log gf-values differed by more than 0.1 dex. Astrophysical log gf-values for the two stars and the average values are listed in Table 5.

The astrophysical log gf-values are compared with the calculated log gf-values in Fig. 7. From this comparison, we excluded the lines at $\lambda\lambda$ 5177.777 (−1.45), 5250.632 (−2.61), 5346.098 (−1.21), and 5420.234 (−1.76) Å, for which the log gf difference between computed and astrophysical log gf-

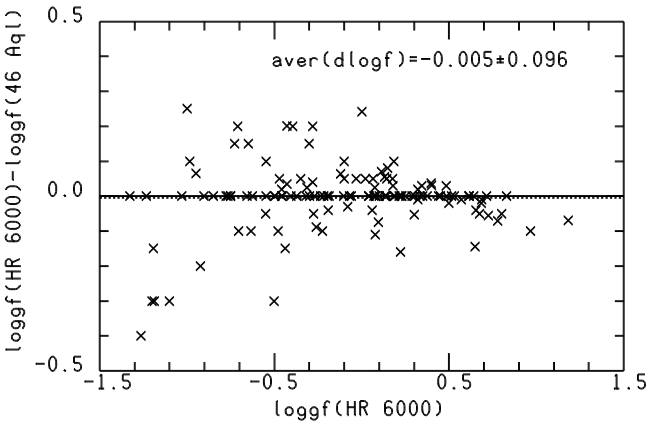

Fig. 6. Comparison of astrophysical log gf-values from HR 6000 and 46 Aql for (^{3}H)4d-(^{3}H)4f transitions of Fe II. The horizontal dashed line indicates the average difference.

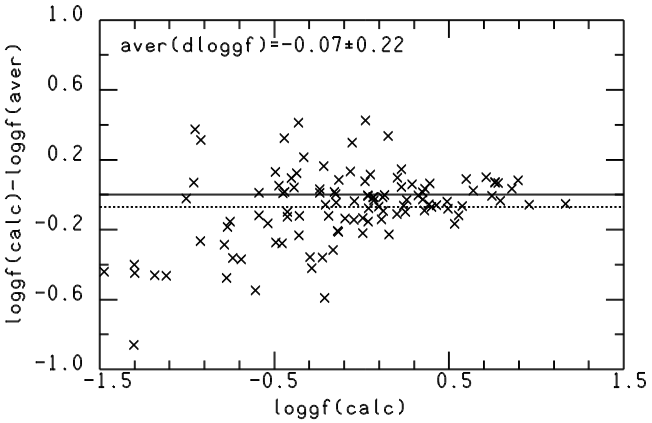

Fig. 7. The calculated log gf-values (calc.) for (^{3}H)4d-(^{3}H)4f transitions of Fe II are compared with astrophysical log gf-values obtained averaging log gf-values from HR 6000 and 46 Aql. The horizontal dashed line indicates the average difference.

values, given in parenthesis, is larger than 1.0 dex. The upper energies of the lines are 122 952.73, 123 026.35, 123 015.40, and 123 251.47 cm^{-1}, respectively. The most probable explanation of these large discrepancies is the presence of some additional unidentified component contributing to the absorption, so that the astrophysical log gf-value is largely overestimated. The mean difference between the two sets of data is -0.07 ± 0.22 dex, indicating that the astrophysical log gf-values are, on average, higher than the computed log gf-values. The differences for the individual lines increase with decreasing log gf, namely with decreasing line intensity. Weak lines are more difficult to be fitted by the synthetic spectrum owing to the contribution of the noise and the non-negligible effect of the position for the continuum.

5.2. More new Fe II identified lines

There are a few other lines that do not belong to the (^{3}H)4d-(^{3}H)4f transitions, that were identified by S. Johansson in HR 6000. They are indicated with a "J" in Table 6. The lines marked with a "K" were then obtained from predicted lines [8] ,[9]tomshttp://kurucz.harvard.edu/atoms/2601/gf2601.lines0600 because of the coincidence of the term of the upper predicted level with the term of a "J" line. Table 6 shows that we fixed two new (^{5}D)6d levels. Some computed log gf-values are much weaker than the astrophysical log gf- values. Some other unknown transition is probably the main component of the observed line so that the astrophysical log gf-value is unreliable.

6. Conclusions

Figure 8 compares the synthetic spectra for HR 6000 computed before and after the study presented in this paper. The interval plotted is an example of the quality of the improvement that we obtained for the whole 5100-5400 Å region. It shows that as many as nine new Fe II lines have been identified within this 10 Å range. Nevertheless, several absorption lines remain unidentified. They are probably Fe II lines whose levels have still to be fixed. A very similar plot was obtained for 46 Aql. We can infer that a large part of the unidentified lines observed in the spectra of B-type stars are due to unknown high-excitation Fe II transitions.

The new lines identified in this paper correspond to high excitation transitions of Fe II with an upper level just below the ionization limit. We fixed 21 new levels of Fe II whose energies range from 122 910.9 cm^{-1} to 123 441.1 cm^{-1}, and added 1700 lines to the Fe II linelist for the range 810 −15011 Å. Furthermore, Johansson (2009) identified in the spectrum of HR 6000 the Fe II lines of the multiplet 4s4d^{8}D − 4s4f^{8}F at 4410 Å. Their lower energy level is near the ionization limit and their upper energy level is above it.

Among the newly identified high-excitation Fe II lines, several have residual flux in HR 6000 and 46 Aql of the order of 0.7 and numerous others are observable as weak absorption lines or parts of blends. The two stars are iron-overabundant stars, but these lines are also present with lower intensity in the UVES spectrum of HD 175640, a B-type peculiar star with an iron underabundance of −0.25 dex with respect to the Sun (Castelli & Hubrig 2004). This implies that Fe II lines from the new high excitation levels contribute to the spectrum of all Population I late B-type stars, even when their abundance is less than solar. The lines are clearly observable in high resolution, high signal-to-noise spectra of slowly rotating stars, while they contribute to the broad observed features in B-type stars with high rotational velocities. In general, they would appear in any object with strong Fe II lines.

We conclude that we have clarified the nature of several unidentified lines observed in the optical spectra of B-type stars and concentrated mostly in the 5000-5400 Å region (see also Wahlgren et al. 2000), but that a large amount of work remains to be done to reproduce stellar observations well. More than 1000 energy levels of Fe II are known, but we have seen that they are not enough. Ignorance of them and of the transitions

[8] http://kurucz.harvard.edu/atoms/2601/gf2601.lines0500

[9] a

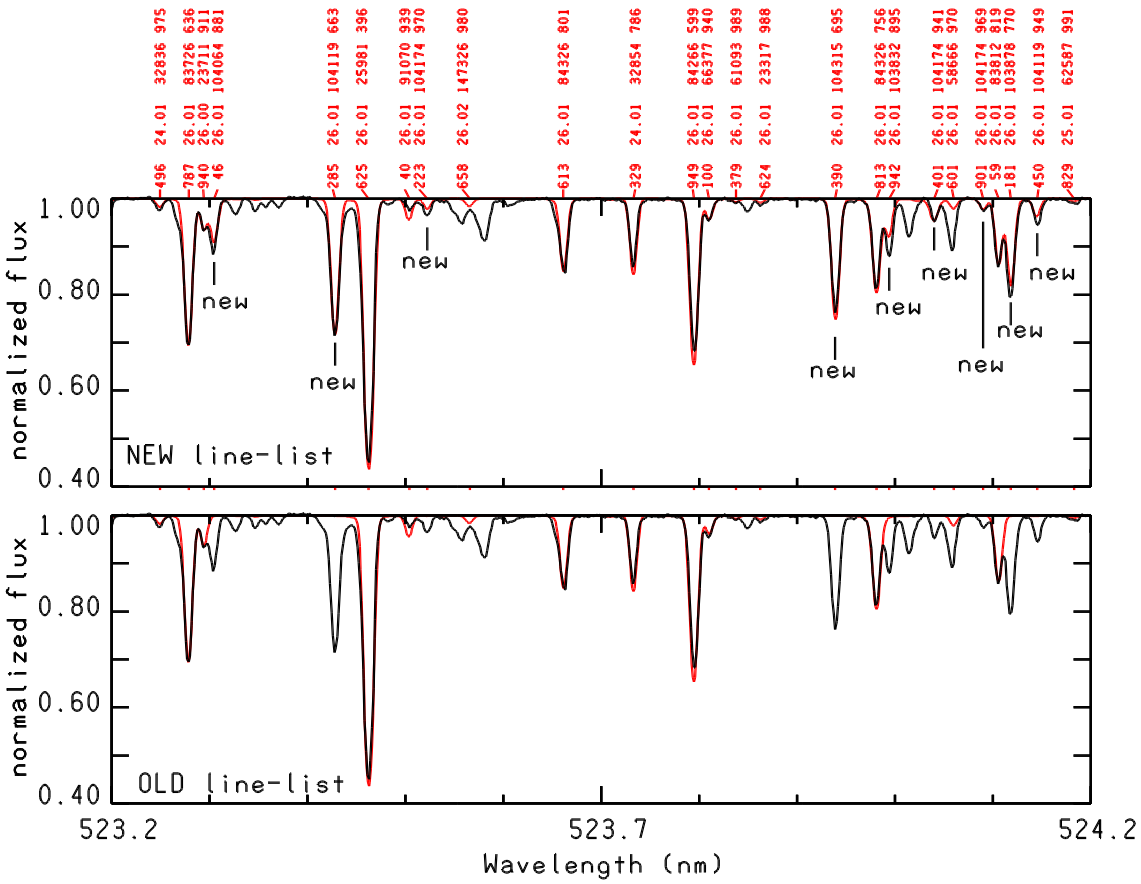

Fig. 8. Comparison of the UVES spectrum of HR 6000 with a synthetic spectrum computed after this study (upper plot) and before this study (lower plot). The black line is the observed spectrum, and the red line is the synthetic spectrum. Nine Fe II lines corresponding to (^{3}H)4d – (^{3}H)4f newly identified transitions are marked in the upper plot. Their calculated log gf-values were used to compute the synthetic spectrum.

involved also remain an outstanding shortcomings affecting the model atmosphere and synthetic spectra computations.

References

Ballester, P., Grosbol, P., Banse, K., Disaro, A., Dorigo, D., Modigliani, A., Pizarro de la Iglesia, J. A., & Boitquin, O. 2000, Proc. SPIE, 4010, 246

Castelli, F. 2005, MSAIS, 8, 44

Castelli, F., & Hubrig, S. 2004, A&A, 425, 263

Castelli, F., & Hubrig, S. 2007, A&A, 475, 1041

Castelli, F., Johansson, S., & Hubrig, S. 2008, Journal of Physics Conference Series, 130, 012003

Cowan, R. D. 1981, The Theory of Atomic Structure and Spectra (Berkeley: Univ. California Press)

Fuhr, J. R., & Wiese, W. L. 2006, Journal of Physical and Chemical Reference Data, 35, 1669

Grevesse, N., & Sauval, A. J. 1998, Space Science Reviews, 85, 161

Hannaford, P., Lowe, R. M., Grevesse, N., Biemont, E., & Whaling, W. 1982, ApJ, 261, 736

Hauck, B., & Mermilliod, M. 1998, A&AS, 129, 431

Johansson, S. 2002, Highlights of Astronomy, 12, 84

Johansson, S. 2009, Physica Scripta, T134, 014013

Johansson, S., & Cowley, C. R. 1984, A&A, 139, 243

Kurucz, R. L. 1993, SYNTHE Spectrum Synthesis Programs and Line Data, CD-ROM, No. 18

Kurucz, R. L. 2005, Memorie della Societa' Astronomica Italiana Supplement, 8, 14

Kurucz, R. L., & Peytremann, E. 1975, SAO Special Report, 362,

Michaud, G. 1970, ApJ, 160, 641

Miller, M. H., Roig, R. A., & Bengtson, R. D. 1971, Phys. Rev. A, 4, 1709

Pickering, J. C., Thorne, A. P., & Perez, R. 2002, ApJS, 138, 247

Raassen, A. J. J., & Uylings, P. H. M. 1998, A&A, 340, 300

Ryabchikova, T. A., & Smirnov, Y. M. 1994, Astronomy Reports, 38, 70

Ryabchikova, T., Wade, G. A., & LeBlanc, F. 2003, Modelling of Stellar Atmospheres, 210, 301

Sadakane, K., et al. 2001, PASJ, 53, 1223

Sbordone, L., Bonifacio, P., Castelli, F., & Kurucz, R. L. 2004, Memorie della Societa Astronomica Italiana Supplement, 5, 93

Sigut, T. A. A., & Landstreet, J. D. 1990, MNRAS, 247, 611

Younger, S. M., Fuhr, Y. R., Martin, G. A., & Wiese, W. L. 1978, Journal of Physical and Chemical Reference Data, 7, 495

Wahlgren, G. M., Dolk, L., Kalus, G., Johansson, S., Litzén, U., & Leckrone, D. S. 2000, ApJ, 539, 908

Warner, B., 1968, MNRAS, 140, 53

Online Material

Appendix A: The Balmer lines of HR 6000 observed on the UVES spectra

Figure A.1 shows the UVES spectra of HR 6000 reduced by the UVES pipeline[10] Data Reduction Software (version 2.5; Ballester et al. 2000) that were used by Castelli & Hubrig (2007) and also in this paper. All spectra are FLUXCAL_SCIENCE products. Those at $\lambda\lambda$ 3290-4520 Å and 4780-5650 Å are flux-calibrated spectra in 10^{-16} erg s^{-1} cm^{-2} A^{-1} corrected for terrestrial extinction. The red spectrum at 5730-7560 Å is in non-physical units 'quasi-ADU' because the flux calibration procedure is not implemented in the reduction software for the REDL and REDU data taken with the red mosaic CCD's. The sizable distortions in UVES spectra make the difficulty in drawing a true continuum over H_γ and H_δ evident. The use of H_β also causes problems because of the position of this line at the left end of the spectrum order. Only H_α does not have significant problems.

Computed spectra from the final ATLAS12 model ([13450,4.3], Sect. 2.2) are also plotted in Fig. A.1 to show the different slopes of the observed and computed continua. The computed fluxes were scaled by a given arbitrary quantity to be roughly overimposed on the UVES spectra.

Appendix B: Lines used for the abundance analysis

Table B.1 lists the lines examined in the spectra of HR 6000 and 46 Aql to derive the stellar abundances. The wording "not obs" is given for lines not present in the spectra, while the wordings "profile" and "blend" are given for lines well observed in the spectra that do not have measurable equivalent widths either because they are too weak to be measurable or because other components affects the line. These wordings also indicate lines for which adequate equivalent widths cannot be computed, as in the cases of Mg II at 4481 Å and most O I lines, which are blends of transitions belonging to the same multiplet. The abundances from the final ATLAS12 models derived from the equivalent widths or from the profiles are given in the Table, as well as upper abundance limits for lines not observed, but predicted at solar abundance by the synthetic spectrum. For Fe I and Fe II, log gf-values were taken from Fuhr & Wiese (2006) (FW06) when available. Otherwise Kurucz's last determination was adopted (Kurucz, 2009), except for Fe II at 5257.119 Å. In this case, the previous values (Kurucz, 2007) produce synthetic profiles in closer agreement with the observations.

[10] http://www.eso.org/ observing/dfo/quality/UVES/pipeline/pipe_reduc.html

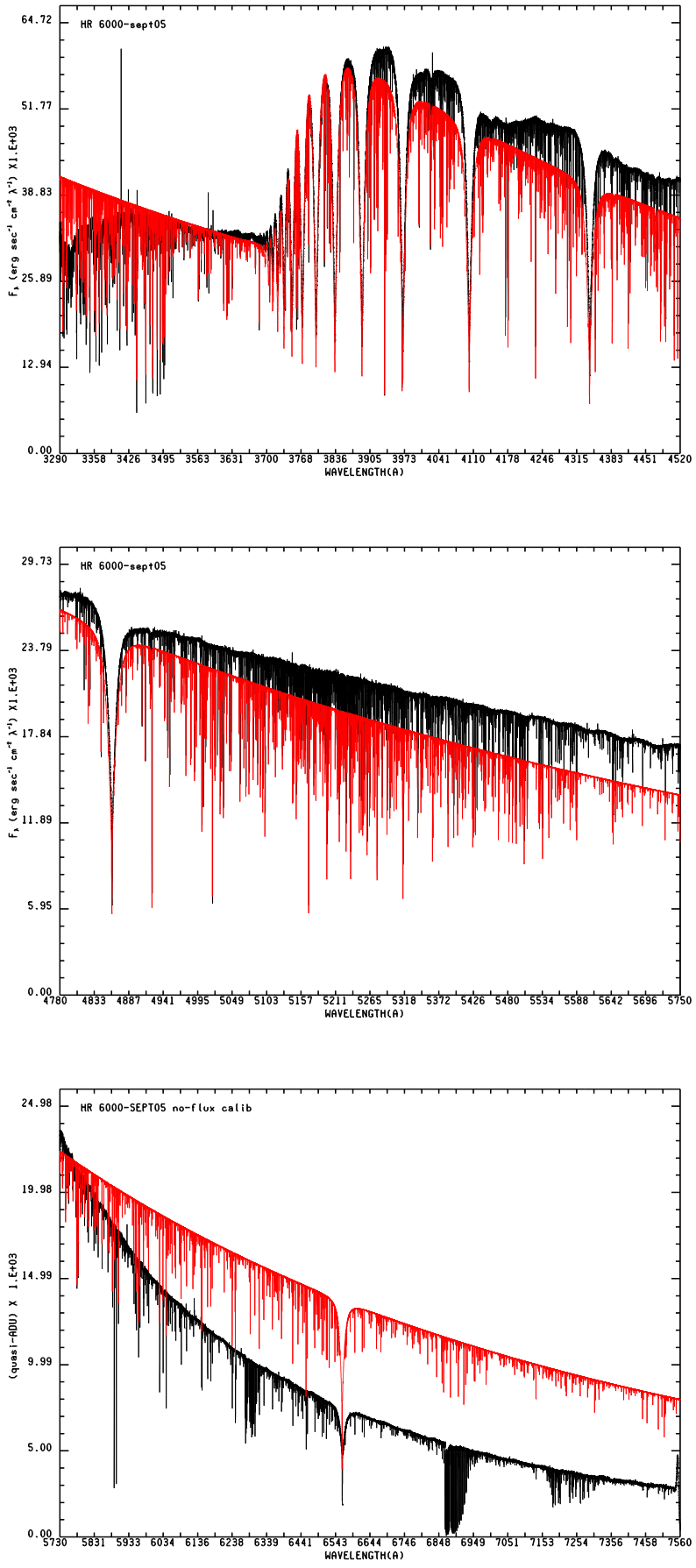

Fig. A.1. The observed UVES spectra of HR 6000 (black line) are plotted together the computed spectra (red line) in order to show the different slopes of the observed and computed continua. The computed fluxes are scaled by a given arbitrary quantity to be roughly overimposed on the UVES spectra. The ATLAS12 final model with parameters $T_{\rm eff}$=13450 K, log g=4.3 was used for the computations.

Table B.1. Analyzed lines in the stellar spectra, measured equivalent widths in mÅ, and relative abundances.He I is not included.

					HR 6000[13450,4.3,AT12]		46 Aql[12560,3.8,AT12]	
Species	λ(Å)	log gf	Ref.[a]	χ_{low}	W(mÅ)	$log(N_{elem}/N_{tot})$	W(mÅ)	$log(N_{elem}/N_{tot})$
Be II	3130.420	−0.170	NIST3	0.00	26.7	−9.78	31.0	−9.91
C II	4267.001	+0.562	NIST3	145549.270	profile	−5.50	profile	−4.75
C II	4267.261	+0.716	NIST3	145550.700	profile	−5.50	profile	−4.75
N I	8680.282	+0.347	NIST3	83364.620	not obs	≤−5.80	not obs	≤−5.50
N I	8683.403	+0.087	NIST3	88317.830	not obs	≤−5.80	not obs	≤−5.50
O I	3947.295	−2.095	NIST3	73768.200	profile	−3.71	profile	−3.71
O I	3947.481	−2.244	NIST3	73768.200	profile	−3.71	profile	−3.71
O I	3947.586	−2.467	NIST3	73768.200	profile	−3.71	profile	−3.71
O I	4368.193	−2.665	NIST3	76794.978	profile	−3.71	profile	−3.51
O I	4368.242	−1.964	NIST3	76794.978	profile	−3.71	profile	−3.51
O I	4368.258	−2.186	NIST3	76794.978	profile	−3.71	profile	−3.51
O I	5329.096	−1.938	NIST3	86625.757	profile	−3.71	profile	−3.46
O I	5329.099	−1.586	NIST3	86625.757	profile	−3.71	profile	−3.46
O I	5329.107	−1.695	NIST3	86625.757	profile	−3.71	profile	−3.46
O I	6155.961	−1.363	NIST3	86625.757	profile	−3.64	profile	−3.46
O I	6155.971	−1.011	NIST3	86625.757	profile	−3.64	profile	−3.46
O I	6155.989	−1.120	NIST3	86625.757	profile	−3.64	profile	−3.46
O I	6156.737	−1.487	NIST3	86627.778	profile	−3.64	profile	−3.43
O I	6156.755	−0.898	NIST3	86627.778	profile	−3.64	profile	−3.43
O I	6156.778	−0.694	NIST3	86627.778	profile	−3.64	profile	−3.43
O I	6455.977	−0.920	NIST3	86631.454	profile	−3.59	profile	−3.43
O I	7002.196	−1.489	NIST3	88631.146	profile	−3.71	H_2O	−−
O I	7002.230	−0.741	NIST3	88631.146	profile	−3.71	H_2O	−−
O I	7002.250	−1.364	NIST3	88631.303	profile	−3.71	H_2O	−−
Ne I	7032.413	−0.249	NIST3	134041.840	noise?	−4.86	noise ?	−4.51
Na I	5688.205	−0.452	NIST3	16973.368	not obs	≤−5.71	profile	−5.65
Na I	5889.950	+0.108	NIST3	0.00	inters.	−−	profile	−5.67
Na I	5895.924	−0.194	NIST3	0.00	inters.	−−	profile	−5.72
Mg II	4481.126	+0.749	NIST3	71490.190	profile	−5.66	profile	−5.45
Mg II	4481.150	−0.553	NIST3	71490.190	profile	−5.66	profile	−5.45
Mg II	4481.325	+0.594	NIST3	71491.063	profile	−5.66	profile	−5.45
Al I	3944.006	−0.638	NIST3	0.000	not obs	≤−7.30	not obs	≤−6.65
Al I	3961.520	−0.336	NIST3	112.061	not obs	≤−7.30	profile	−6.65
Al II	7042.083	+0.340	NIST3	91274.500	noise ?	≤−7.30	noise ?	≤−7.40
Al II	7056.712	+0.110	NIST3	91274.500	noise ?	≤−7.30	noise ?	≤−7.00
Si II	3853.665	−1.341	NIST3	55309.350	not obs	−−	31.8	−5.62
Si II	3862.595	−0.406	NIST3	55325.180	not obs	−−	71.8	−5.68
Si II	3862.595	−0.757	NIST3	55309.350	profile	−7.35	62.6	−5.53
P II	4044.576	+0.481	K,MRB	107360.250	45.3	−4.42	19.9	−5.16
P II	4062.149	−0.585	K,MRB	103339.140	8.6	−4.79	2.4	−5.45
P II	4127.559	−0.110	K,KP	103667.860	25.2	−4.54	9.3	−5.21
P II	4160.623	−0.410	K,KP	103339.140	9.4	−4.90	7.6	−5.03
P II	4244.622	−0.308	K,MRB	107360.250	9.6	−4.78	2.6	−5.46
P II	4288.606	−0.630	K,MRB	101635.690	7.0	−4.88	blend	−−
P II	4420.712	−0.329	NIST3	88893.220	40.1	−4.51	19.4	−5.18
P II	4452.472	−0.194	K,MRB	105302.170	19.9	−4.48	6.9	−5.13
P II	4463.027	+0.026	K,MRB	105549.670	25.6	−4.52	9.1	−5.19
P II	4466.140	−0.560	NIST3	105549.670	9.8	−4.57	2.2	−5.32
P II	4468.000	−0.208	K,MRB	105244.060	24.0	−4.35	blend	−−
P II	4475.270	+0.440	NIST3	105549.670	36.8	−4.63	16.2	−5.25
P II	4483.693	−0.431	NIST3	105302.370	10.0	−4.69	2.3	−5.43
P II	4499.230	+0.470	NIST3	107922.930	38.0	−4.44	blend	−−
P II	5296.077	−0.160	NIST3	87124.600	56.3	−4.15	33.9	−4.74
P II	5316.055	−0.294	NIST3	86743.960	47.9	−4.31	28.3	−4.82
P II	5344.729	−0.390	NIST3	86597.550	45.6	−4.28	25.7	−4.81
P II	5386.895	−0.520	NIST3	86743.960	51.8	−3.98	25.6	−4.67
P II	5425.880	+0.180	NIST3	87124.600	71.8	−4.22	47.4	−4.71

Table B.1. cont.

					HR 6000[13450,4.3,AT12]		46 Aql[12560,3.8,AT12]	
Species	λ(Å)	log gf	Ref.[a]	χ_{low}	W(mÅ)	$log(N_{elem}/N_{tot})$	W(m)	$log(N_{elem}/N_{tot})$
P II	6024.178	+0.137	NIST3	86743.960	69.8	−4.04	45.7	−4.57
P II	6034.039	−0.220	NIST3	86597.550	52.6	−4.10	29.4	−4.70
P II	6043.084	+0.416	NIST3	87124.600	81.1	−4.05	55.5	−4.57
P III	4059.312	−0.051	NIST3	116885.870	11.1	−4.97	2.5	−5.87
P III	4080.089	−0.306	NIST3	116874.560	5.5	−5.21	not ob	−−
P III	4222.198	+0.210	NIST3	117835.950	19.5	−5.45	not obs	−−
P III	4246.720	−0.120	NIST3	117835.950	10.6	−4.78	not obs	−−
S II	4162.665	+0.777	NIST3	128599.160	2.0	−6.26	5.3	−5.74
Cl I	4794.556	+0.400	NIST3	107879.660	not obs	≤−7.24	not obs	≤−7.04
Ca I	4226.728	+0.244	NIST3	0.000	profile	>−5.68	profile	>−5.98
Ca II	3933.663	+0.135	NIST3	0.000	profile	−5.68	profile	−5.98
Ca II	3968.469	−0.180	NIST3	0.000	profile	−5.68	profile	−5.98
Sc II	4246.822	+0.242	NIST3	2540.950	blend	−−	blend	−−
Sc II	4314.083	−0.100	NIST3	4987.790	not obs	≤ −9.50	not obs	≤−9.50
Ti II	4053.821	−1.130	PTP	15265.620	6.4	−6.40	11.1	−6.46
Ti II	4163.644	−0.130	PTP	20891.660	19.3	−6.51	30.4	−6.50
Ti II	4287.873	−1.790	PTP	8710.440	3.5	−6.38	6.1	−6.49
Ti II	4290.215	−0.850	PTP	9395.710	15.6	−6.55	28.3	−6.52
Ti II	4294.094	−0.930	PTP	9744.250	16.5	−6.47	28.3	−6.48
Ti II	4300.042	−0.440	PTP	9518.060	30.2	−6.52	45.2	−6.49
Ti II	4301.922	−1.150	PTP	9363.620	8.6	−6.56	17.1	−6.55
Ti II	4367.652	−0.860	PTP	20891.660	5.7	−6.42	9.9	−6.46
Ti II	4395.031	−0.540	PTP	8744.250	29.2	−6.49	45.2	−6.43
Ti II	4399.765	−1.190	PTP	9975.920	3.3	−6.94	17.2	−6.48
Ti II	4411.072	−0.670	PTP	24961.030	5.0	−6.45	10.1	−6.40
Ti II	4417.714	−1.190	PTP	9395.710	8.8	−6.51	16.4	−6.54
Ti II	4418.331	−1.970	PTP	9975.920	2.4	−6.31	3.5	−6.50
Ti II	4443.810	−0.720	PTP	8710.440	22.3	−6.50	37.1	−6.47
Ti II	4450.482	−1.520	PTP	8744.250	5.5	−6.45	11.5	−6.44
Ti II	4464.448	−1.810	PTP	9363.620	3.1	−6.40	6.8	−6.38
Ti II	4468.492	−0.620	NIST3	9118.260	25.6	−6.50	39.6	−6.50
Ti II	4488.325	−0.510	PTP	25192.710	7.0	−6.44	12.4	−6.44
Ti II	4501.270	−0.770	PTP	8997.710	23.0	−6.41	37.6	−6.39
Ti II	4805.085	−1.120	NIST3	16625.110	7.2	−6.28	14.5	−6.27
Ti II	4911.195	−0.610	PTP	25192.790	5.4	−6.45	10.7	−6.42
V II	3093.105	+0.530	K,NBS	3162.800	blend	≤−9.14	noise ?	≤−8.94
V II	3102.289	+0.410	K,NBS	2968.220	not obs	≤−9.14	noise	≤−8.94
V II	3110.695	+0.300	K,NBS	2808.720	blend	≤−9.14	blend	≤−8.94
V II	3113.376	+0.180	K,NBS	2687.010	not obs	≤−9.14	not obs	≤−8.94
V II	3125.276	+0.070	K,NBS	2604.820	blend	≤−9.14	blend	−8.94
Cr II	4812.337	−1.800	NIST3	31168.580	3.7	−6.21	not obs	−−
Cr II	4824.127	−0.970	SL	31219.350	26.4	−5.98	blend	−−
Cr II	4836.229	−2.000	SL	31117.390	3.9	−5.99	not obs	−−
Cr II	5237.329	−1.160	NIST3	32854.310	12.5	−6.16	1.5	−7.48
Cr II	5246.768	−2.460	NIST3	29951.880	1.2	−6.14	not obs	−−
Mn II	3441.988	−0.270	NIST3	14325.860	85.3	−4.92 (−5.00)[b]	74.5	−5.48 (−5.35)[b]
Mn II	3460.316	−0.540	NIST3	14593.820	74.5	−4.91 (−5.00)	60.2	−5.65 (−5.65)
Mn II	3482.905	−0.740	NIST3	14781.190	65.3	−4.98 (−5.00)	53.0	−5.70 (−5.65)
Mn II	3488.677	−0.860	NIST3	14901.180	65.7	−4.85 (−4.85)	52.5	−5.60 (−5.60)
Mn II	3495.833	−1.220	NIST3	14959.840	55.3	−4.85 (−4.85)	42.2	−5.65 (−5.65)
Mn II	3496.809	−1.690	NIST3	14781.190	38.1	−5.09 (−5.00)	27.0	−5.87 (−5.90)
Mn II	3497.526	−1.330	NIST3	14901.180	47.7	−5.05 (−4.90)	35.5	−5.84 (−5.85)
Mn II	3917.318	−1.169	K03Mn	55759.270	4.9	−5.61 (−5.65)	2.8	−6.09 (−6.17)
Mn II	4363.258	−1.929	K03Mn	44899.820	4.2	−5.49 (−5.58)	2.3	−6.03 (−6.15)
Mn II	4365.219	−1.339	K03Mn	44899.820	4.7	−5.59 (−5.63)	3.1	−6.02 (−6.07)
Mn II	4478.635	−0.942	K03Mn	53597.130	8.2	−5.68 (−5.63)	5.0	−6.16 (−6.15)
Fe I	3581.193	+0.406	FW06	6928.27	17.3	−3.67	19.2	−3.86
Fe I	3618.768	−0.003	FW06	7985.78	8.0	−3.73	10.3	−3.88
Fe I	4005.242	−0.610	FW06	12560.93	6.6	−3.59	6.4	−3.94

Table B.1. cont.

					HR 6000[13450,4.3,AT12]		46 Aql[12560,3.8,AT12]	
Species	λ(Å)	log gf	Ref.[a]	χ_{low}	W(mÅ)	$log(N_{elem}/N_{\rm tot})$	W(mÅ)	$log(N_{elem}/N_{\rm tot})$
Fe I	4071.738	−0.022	FW06	12698.55	15.4	−3.71	17.0	−3.99
Fe I	4202.029	−0.708	FW06	11976.24	4.5	−3.71	5.7	−3.93
Fe I	4219.360	+0.000	FW06	28819.95	4.0	−3.55	4.4	−3.78
Fe I	4235.936	−0.341	FW06	19562.44	4.9	−3.62	5.9	−3.84
Fe I	4271.760	−0.164	FW06	11976.24	14.7	−3.66	16.4	−3.93
Fe I	4383.545	+0.200	FW06	11976.24	25.2	−3.67	27.6	−3.95
Fe I	4404.750	−0.142	FW06	12560.93	18.6	−3.51	18.0	−3.87
Fe I	4415.122	−0.615	FW06	12968.55	6.2	−3.61	8.0	−3.81
Fe I	5324.179	−0.103	FW06	25899.99	blend	−−	3.3	−3.98
Fe I	5364.871	+0.228	FW06	35856.40	2.4	−3.61	2.2	−3.92
Fe I	5369.962	+0.536	FW06	35257.32	5.0	−3.62	4.3	−3.95
Fe I	5410.910	+0.398	FW06	36079.37	2.6	−3.74	2.9	−3.94
Fe I	5424.068	+0.580	FW06	34843.95	blend	−−	5.0	−3.94
Fe I	5615.644	+0.050	FW06	26874.55	blend	−−	3.9	−3.99
Fe II	3906.035	−1.700	FW06	44929.55	42.8	−3.82	43.7	−4.02
Fe II	3914.503	−4.370	FW06	13473.41	18.1	−3.60	22.4	−3.80
Fe II	3935.962	−1.720	FW06	44915.05	43.3	−3.79	44.1	−3.99
Fe II	3938.290	−4.070	FW06	13471.41	37.1	−3.35	31.7	−3.83
Fe II	3945.210	−4.440	FW06	13673.18	14.7	−3.65	18.1	−3.85
Fe II	4122.668	−3.300	FW06	20830.58	33.4	−3.82	36.8	−4.03
Fe II	4128.748	−3.580	FW06	20830.58	23.6	−3.82	27.9	−4.00
Fe II	4178.862	−2.440	FW06	20830.58	58.3	−3.93	61.7	−4.11
Fe II	4258.154	−3.480	FW06	21812.05	26.6	−3.78	29.7	−3.99
Fe II	4273.326	−3.300	FW06	21812.05	32.6	−3.79	39.6	−3.90
Fe II	4296.572	−2.930	FW06	21812.05	44.5	−3.82	50.1	−3.95
Fe II	4303.176	−2.610	FW06	21812.05	57.6	−3.74	63.1	−3.86
Fe II	4369.411	−3.580	FW06	22409.85	21.5	−3.80	25.5	−3.98
Fe II	4413.601	−4.190	FW06	21581.64	10.4	−3.66	13.7	−3.81
Fe II	4416.830	−2.600	FW06	22409.85	56.7	−3.75	59.3	−3.96
Fe II	4491.405	−2.640	FW06	23031.30	49.8	−3.88	53.5	−4.06
Fe II	4508.288	−2.350	FW06	23031.30	66.2	−3.68	70.1	−3.84
Fe II	4515.339	−2.360	FW06	23939.36	57.8	−3.86	61.3	−4.04
Fe II	4520.224	−2.620	FW06	22637.21	54.4	−3.78	no spectra	−−
Fe II	4522.634	−1.990	FW06	22939.36	68.7	−3.97	no spectra	−−
Fe II	4923.927	−1.210	FW06	23317.63	100.8	−3.91	blend	−−
Fe II	4993.358	−3.680	FW06	22637.20	19.6	−3.74	23.2	−3.93
Fe II	5004.188	+0.482	K09	82853.66			47.6	−3.88
Fe II	5006.840	−0.281	K09	83713.53			20.4	−3.90
Fe II	5007.450	−0.382	K09	83726.37			16.4	−3.94
Fe II	5010.060	−0.808	K09	83726.37			10.1	−3.80
Fe II	5011.026	−1.177	K09	83726.37			3.6	−3.95
Fe II	5018.440	−1.350	FW06	23317.63	111.7	−3.57	116.7	−3.77
Fe II	5022.419	−0.052	K09	83459.67			23.6	−4.03
Fe II	5026.798	−0.235	K09	83136.46			22.0	−3.92
Fe II	5030.631	+0.431	FW06	82978.68	50.7	−3.69	43.2	−3.95
Fe II	5032.704	+0.143	K09	83812.30			30.9	−3.97
Fe II	5035.700	+0.630	FW06	82978.68	59.7	−3.64	51.6	−3.90
Fe II	5036.713	−0.527	K09	83812.30			13.0	−3.94
Fe II	5045.108	−0.116	K09	83136.46			26.8	−3.88
Fe II	5060.249	−0.479	K09	84266.54			12.7	−3.97
Fe II	5062.927	−1.166	K09	83136.46			7.0	−3.68
Fe II	5067.890	−0.173	K09	83308.19			22.4	−3.95
Fe II	5070.583	−0.865	K09	83308.19			6.6	−3.99
Fe II	5070.895	+0.262	K09	83136.46			37.9	−3.92
Fe II	5075.760	+0.233	K09	84326.92			33.3	−3.95
Fe II	5076.597	−0.749	K09	83713.53			8.8	−3.95
Fe II	5081.898	−0.689	K09	83713.53			8.3	−4.02

Table B.1. cont.

					HR 6000[13450,4.3,AT12]		46 Aql[12560,3.8,AT12]	
Species	λ(Å)	log gf	Ref.[a]	χ_{low}	W(mÅ)	$log(N_{elem}/N_{\rm tot})$	W(mÅ)	$log(N_{elem}/N_{\rm tot})$
Fe II	5086.306	−0.472	K09	83990.06			14.7	−3.90
Fe II	5089.214	−0.014	K09	83308.19			27.0	−3.96
Fe II	5093.783	−0.703	K09	83726.37			12.7	−3.77
Fe II	5117.032	−0.129	K09	84131.58			22.0	−3.96
Fe II	5132.669	−4.090	FW06	22637.20	17.5	−3.40	14.0	−3.83
Fe II	5140.692	−0.822	K09	83990.06			9.9	−3.78
Fe II	5143.875	+0.054	K09	84266.54			21.6	−4.14
Fe II	5144.352	+0.307	FW06	84424.37	40.1	−3.73	32.8	−4.03
Fe II	5169.033	−0.870	FW06	23317.63	115.1	−4.01	121.0	−4.19
Fe II	5180.312	+0.002	K09	83812.30			26.9	−3.94
Fe II	5199.118	+0.054	K09	83713.53			30.3	−3.87
Fe II	5200.798	−0.390	K09	83812.30			17.4	−3.87
Fe II	5203.634	−0.088	K09	83812.30			25.9	−3.88
Fe II	5218.841	−0.250	K09	83726.37			23.6	−3.85
Fe II	5219.920	−0.628	K09	84870.86			10.3	−3.89
Fe II	5222.350	−0.332	K09	84844.82			15.0	−3.96
Fe II	5223.802	−0.546	K09	83713.53			14.6	−3.83
Fe II	5224.404	−0.581	K09	83990.06			12.5	−3.87
Fe II	5234.625	−2.210	FW06	25981.63	69.6	−3.54	71.0	−3.76
Fe II	5237.949	+0.103	K09	84266.54			29.8	−3.90
Fe II	5245.455	−0.502	K09	84326.92			13.6	−3.88
Fe II	5247.956	+0.550	FW06	84938.18	46.2	−3.74	39.7	−4.01
Fe II	5257.119	+0.115	K07	84685.20			26.7	−4.00
Fe II	5265.985	−0.936	K09	84035.12			9.3	−3.68
Fe II	5270.029	−0.097	K09	84710.70			18.0	−4.08
Fe II	5272.397	−2.010	FW06	48039.09	35.0	−3.51	35.4	−3.71
Fe II	5276.002	−1.900	FW06	25805.33	67.0	−3.93	71.7	−4.07
Fe II	5284.109	−3.200	FW06	23317.63	38.2	−3.63	40.6	−3.86
Fe II	5291.661	+0.561	K09	84527.76			42.8	−3.95
Fe II	5306.182	+0.044	FW06	84870.87	30.4	−3.70	26.7	−3.91
Fe II	5315.083	−0.422	K09	85048.61			13.2	−3.93
Fe II	5316.615	−1.780	FW06	25428.78	79.9	−3.71	81.9	−3.93
Fe II	5318.055	−0.177	K09	84527.76			22.3	−3.85
Fe II	5355.421	−0.203	K09	84685.20			13.2	−4.17
Fe II	5358.872	−0.130	K09	84685.20			14.8	−4.17
Fe II	5359.237	−1.112	K09	84710.70			7.2	−3.59
Fe II	5366.210	−0.549	K09	84710.70			16.4	−3.68
Fe II	5425.257	−3.390	FW06	25805.33	27.8	−3.59	30.2	−3.81
Fe II	5430.003	+0.427	FW06	85462.86			36.7	−3.92
Fe II	5444.386	−0.153	K09	85495.32			19.5	−3.90
Fe II	5451.316	−0.756	K09	84685.20			7.1	−3.95
Fe II	5465.932	+0.348	FW06	85679.70	42.3	−3.58	35.6	−3.86
Fe II	5472.855	−0.723	K09	84685.20			10.5	−3.77
Fe II	5475.826	−0.129	K09	84685.20			19.7	−3.96
Fe II	5488.776	−0.468	K09	85462.86			13.3	−3.84
Fe II	5492.398	−0.127	K09	84685.20			25.1	−3.78
Fe II	5493.830	+0.259	FW06	84685.20	37.7	−3.68	32.5	−3.93
Fe II	5502.670	−0.179	K09	85184.73			21.2	−3.83
Fe II	5534.847	−2.860	FW06	26170.18	50.5	−3.44	51.1	−3.70
Co II	3501.708	−1.111	K06	17771.506	not obs	−−	not obs	≤ -8.02
Co II	4160.657	−1.751	K06	27484.371	blend	−−	blend	−−
Ni II	4067.031	−1.834	K03Ni	32499.530	9.9	−6.24	9.8	−6.47
Cu II	4909.734	+0.790	K03Cu	115568.985	not obs	−−	3.1	−6.26
Cu II	4931.698	+0.704	K03Cu	115662.550	not obs	−−	2.7	−6.22
Zn I	4810.528	−0.137	K,WAR	32890.352	not obs	−−	5.1	−5.85
Zn II	4911.625	+0.540	NIST3	96909.740	not obs	−−	23.0	−5.76

Table B.1. cont.

					HR 6000[13450,4.3,AT12]		46 Aql[12560,3.8,AT12]	
Species	λ(Å)	log gf	Ref.[a]	χ_{low}	W(mÅ)	$log(N_{elem}/N_{\rm tot})$	W(mÅ)	$log(N_{elem}/N_{\rm tot})$
Ga II	4255.722	+0.634	RS94	113842.190	not obs	−−	not obs	−−
Ga II	6334.069	+1.000	RS94	102944.550	not obs	−−	not obs	−−
As II	5105.58	−−	−−	81508.925	not obs	−−	4.0	−−
As II	5107.55	−−	−−	82819.214	not obs	−−	blend	−−
As II	5231.38	−−	−−	79128.330	not obs	−−	3.2	−−
As II	5331.23	−−	−−	81508.925	not obs	−−	9.4	−−
As II	5497.73	−−	−−	78730.893	not obs	−−	blend	−−
As II	5558.09	−−	−−	79128.330	not obs	−−	9.4	−−
As II	5651.32	−−	−−	81508.925	not obs	−−	11.0	−−
As II	6110.07	−−	−−	83819.214	not obs	−−	3.3	−−
As II	6170.27	−−	−−	79128.330	not obs	−−	blend	−−
Sr II	4077.709	+0.151	NIST3	0.000	not obs	−−	not obs	−−
Y II	3950.349	−0.490	K,HL	840.213	profile	−8.60	4.2	−8.20
Y II	4883.682	+0.070	K,HL	8743.316	profile	−8.60	7.3	−8.03
Y II	4900.120	−0.090	K,HL	8328.041	profile	−8.60	5.5	−8.04
Xe II	4844.330	+0.491	NIST3	93068.440	28.8	−5.23	17.5	−5.81
Hg II	3983.890	−1.510	NIST3	35514.000	profile	−8.20	profile	−7.10

[a] (NIST3) NIST Atomic Spectra Database, version 3 at http://physics.nist.gov;
(FW06) Fuhr & Wiese (2006);
(PTP) Pickering et al. (2002);
(RS94) Ryabchikova & Smirnov (1994);
(SL) Sigut & Landstreet (1990);
K03Mn: http://kurucz.harvard.edu/atoms/2501/gf2501.pos;
K03Ni: http://kurucz.harvard.edu/atoms/2801/gf2801.pos;
K03Cu: http://kurucz.harvard.edu/atoms/2901/gf2901.pos;
K06: http://kurucz.harvard.edu/atoms/2701/gf2701.pos;
K07: http://kurucz.harvard.edu/atoms/2601/gf2601.pos, 2007 version, no longer available. The log gf gives better agreement with the observations than the K09 new determination;
K09: http://kurucz.harvard.edu/atoms/2601/gf2601.pos,January 2009 version;
"K" before another log gf source means that the log gf is from Kurucz files available at http://kurucz.harvard.edu/linelists/gf100/; (HL) Hannaford et al. (1982);(KP) Kurucz & Peytremann (1975); (MRB) Miller et al. (1971); (NBS) Younger et al. (1979); (WAR) Warner (1968).
[b] The abundances given in parenthesis were derived from line profiles. All computed line profiles include hyperfine components, except for that at 3917.318 Å.

Table 4. Astrophysical log gf-values for a sample of (^{5}D)4d−(^{5}D)4f lines of Fe II observed in HR 6000 and 46 Aql. The values of log gf from the two stars are averaged and compared with experimental log gf-values from Johansson (2002) and calculated log gf-values from Kurucz (2009)(K09)(footnote 7) and from Raassen & Uylings (1998) (RU98).

λ(Å)	transition		χ_{low}(cm^{-1})	χ_{up}(cm^{-1})	loggf					
					exp	HR 6000	46 Aql	Aver	K09	RU98
4883.292	(^{5}D)4d e^{6}F$_{11/2}$	(^{5}D)4f 3[5]$_{11/2}$	82853.656	103325.927	−0.521	−0.673	−0.643	−0.658	−0.651	−0.601
4913.295	(^{5}D)4d e^{6}F$_{9/2}$	(^{5}D)4f 3[5]$_{11/2}$	82978.668	103325.927	0.016	−0.014	0.006	−0.004	−0.069	0.050
4990.509	(^{5}D)4d e^{6}F$_{5/2}$	(^{5}D)4f 3[4]$_{7/2}$	83308.195	103340.652		0.118	0.168	0.143	0.161	0.195
5001.953	(^{5}D)4d e^{6}F$_{11/2}$	(^{5}D)4f 4[6]$_{13/2}$	82853.656	102840.269	0.933	0.963	0.983	0.973	0.884	0.916
5004.188	(^{5}D)4d e^{6}F$_{11/2}$	(^{5}D)4f 4[5]$_{11/2}$	82853.656	102831.344		0.574	0.594	0.584	0.482	0.504
5006.840	(^{5}D)4d ^{6}D$_{7/2}$	(^{5}D)4f 2[4]$_{9/2}$	83713.534	103680.640		−0.265	−0.300	−0.282	−0.281	−0.362
5007.450	(^{5}D)4d ^{6}D$_{9/2}$	(^{5}D)4f 2[5]$_{11/2}$	83726.367	103691.045		−0.390	−0.390	−0.390	−0.382	−0.460
5010.061	(^{5}D)4d ^{6}D$_{9/2}$	(^{5}D)4f 2[4]$_{9/2}$	83726.367	103680.640		−0.693	−0.710	−0.701	−0.808	−0.694
5011.026	(^{5}D)4d ^{6}D$_{9/2}$	(^{5}D)4f 2[3]$_{7/2}$	83726.367	103676.798		−1.165	−1.185	−1.175	−1.177	−1.183
5022.419	(^{5}D)4d e^{6}F$_{3/2}$	(^{5}D)4f 3[3]$_{5/2}$	83459.674	103364.847		−0.142	−0.162	−0.152	−0.052	−0.072
5026.798	(^{5}D)4d e^{6}F$_{7/2}$	(^{5}D)4f 4[2]$_{5/2}$	83136.462	103024.293		−0.287	−0.257	−0.272	−0.235	−0.444
5030.631	(^{5}D)4d e^{6}F$_{9/2}$	(^{5}D)4f 4[5]$_{9/2}$	82978.668	102851.345		0.361	0.401	0.381	0.428	0.431
5032.704	(^{5}D)4d ^{6}D$_{5/2}$	(^{5}D)4f 2[3]$_{7/2}$	83812.304	103676.798		0.050	0.060	0.055	0.143	0.076
5035.700	(^{5}D)4d e^{6}F$_{9/2}$	(^{5}D)4f 4[5]$_{11/2}$	82978.668	102831.344		0.557	0.647	0.602	0.611	0.632
5036.713	(^{5}D)4d ^{6}D$_{5/2}$	(^{5}D)4f 2[2]$_{5/2}$	83812.304	103660.987		−0.546	−0.546	−0.546	−0.527	−0.565
5045.108	(^{5}D)4d e^{6}F$_{7/2}$	(^{5}D)4f 4[3]$_{5/2}$	83136.462	102952.122		−0.150	−0.130	−0.140	−0.116	−0.002
5060.249	(^{5}D)4d ^{6}P$_{7/2}$	(^{5}D)4f 0[3]$_{7/2}$	84266.544	104022.912		−0.555	−0.555	−0.555	−0.479	−0.650
5062.927	(^{5}D)4d e^{6}F$_{7/2}$	(^{5}D)4f 4[4]$_{9/2}$	83136.462	102882.375		−0.906	−0.906	−0.906	−1.166	−1.113
5067.890	(^{5}D)4d e^{6}F$_{5/2}$	(^{5}D)4f 4[2]$_{3/2}$	83308.195	103034.770		−0.249	−0.219	−0.234	−0.173	−0.078
5070.583	(^{5}D)4d e^{6}F$_{5/2}$	(^{5}D)4f 4[2]$_{5/2}$	83308.195	103024.293		−0.914	−0.914	−0.914	−0.865	−1.674
5070.895	(^{5}D)4d e^{6}F$_{7/2}$	(^{5}D)4f 4[5]$_{9/2}$	83136.462	102851.345		0.189	0.249	0.219	0.262	0.268
5075.760	(^{5}D)4d ^{6}P$_{5/2}$	(^{5}D)4f 0[3]$_{7/2}$	84326.918	104022.912		0.105	0.150	0.127	0.233	0.184
5076.597	(^{5}D)4d ^{6}D$_{7/2}$	(^{5}D)4f 3[2]$_{5/2}$	83713.534	103406.278		−0.770	−0.790	−0.780	−0.749	−0.924
5081.898	(^{5}D)4d ^{6}D$_{7/2}$	(^{5}D)4f 3[3]$_{7/2}$	83713.534	103385.735		−0.783	−0.783	−0.783	−0.689	−1.062
5083.503	(^{5}D)4d e^{6}F$_{3/2}$	(^{5}D)4f 4[1]$_{1/2}$	83459.674	103125.669		−0.870	−0.900	−0.885	−0.788	−0.752
5086.306	(^{5}D)4d ^{6}D$_{3/2}$	(^{5}D)4f 2[2]$_{3/2}$	83990.059	103645.211		−0.470	−0.470	−0.470	−0.472	−0.419
5089.214	(^{5}D)4d e^{6}F$_{5/2}$	(^{5}D)4f 4[3]$_{5/2}$	83308.195	102952.122		−0.081	−0.046	−0.063	−0.014	0.013
5093.783	(^{5}D)4d ^{6}D$_{9/2}$	(^{5}D)4f 4[5]$_{9/2}$	83726.367	103352.673		−0.550	−0.570	−0.560	−0.703	−0.959
5100.734	(^{5}D)4d ^{6}D$_{9/2}$	(^{5}D)4f 4[5]$_{11/2}$	83726.367	103352.927	0.671				0.703	0.718
5117.032	(^{5}D)4d ^{6}D$_{1/2}$	(^{5}D)4f 2[1]$_{3/2}$	84131.575	103668.714		−0.184	−0.194	−0.189	−0.129	−0.039
5140.689	(^{5}D)4d ^{6}D$_{3/2}$	(^{5}D)4f 3[1]$_{1/2}$	83990.059	103437.280		−0.639	−0.674	−0.656	−0.822	−1.190
5143.875	(^{5}D)4d ^{6}P$_{7/2}$	(^{5}D)4f 2[5]$_{9/2}$	84266.544	103701.729		−0.206	−0.178	−0.192	0.054	−0.205
5144.352	(^{5}D)4d ^{6}P$_{3/2}$	(^{5}D)4f 1[2]$_{5/2}$	84424.376	103857.755		0.162	0.172	0.167	0.260	0.307
5149.465	(^{5}D)4d ^{6}P$_{7/2}$	(^{5}D)4f 2[4]$_{9/2}$	84266.544	103680.640		0.319	0.389	0.354	0.405	0.553
5180.312	(^{5}D)4d ^{6}D$_{5/2}$	(^{5}D)4f 4[1]$_{3/2}$	83812.304	103110.786		−0.019	0.010	−0.004	0.002	−0.088
5199.188	(^{5}D)4d ^{6}D$_{7/2}$	(^{5}D)4f 4[3]$_{7/2}$	83713.534	102942.208		0.082	0.100	0.091	0.054	0.122
5200.798	(^{5}D)4d ^{6}D$_{5/2}$	(^{5}D)4f 4[2]$_{3/2}$	83812.304	103034.770		−0.328	−0.318	−0.323	−0.390	−0.036
5203.634	(^{5}D)4d ^{6}D$_{5/2}$	(^{5}D)4f 4[2]$_{5/2}$	83812.304	103024.293		−0.073	−0.049	−0.061	−0.088	−0.115
5218.841	(^{5}D)4d ^{6}D$_{9/2}$	(^{5}D)4f 4[4]$_{9/2}$	83726.367	102882.375		−0.160	−0.115	−0.137	−0.250	−0.165
5219.920	(^{5}D)4d f^{4}D$_{5/2}$	(^{5}D)4f 0[3]$_{7/2}$	84870.864	104022.912		−0.590	−0.590	−0.590	−0.628	−0.550
5222.350	(^{5}D)4d e^{6}G$_{5/2}$	(^{5}D)4f 1[3]$_{5/2}$	84844.819	103987.951		−0.355	−0.355	−0.355	−0.332	−0.281
5223.802	(^{5}D)4d ^{6}D$_{7/2}$	(^{5}D)4f 4[5]$_{9/2}$	83713.534	102851.345		−0.486	−0.476	−0.481	−0.546	−0.506
5224.404	(^{5}D)4d ^{6}D$_{3/2}$	(^{5}D)4f 4[1]$_{1/2}$	83990.059	103125.669		−0.519	−0.519	−0.519	−0.581	−0.428
5227.487	(^{5}D)4d e^{6}G$_{11/2}$	(^{5}D)4f 3[6]$_{13/2}$	84296.833	103421.165	0.831	0.806	0.831	0.818	0.811	0.846
5237.949	(^{5}D)4d ^{6}P$_{7/2}$	(^{5}D)4f 3[5]$_{9/2}$	84266.544	103352.673		0.035	0.065	0.050	0.103	0.104
5245.455	(^{5}D)4d ^{6}P$_{5/2}$	(^{5}D)4f 3[3]$_{7/2}$	84326.918	103385.735		−0.504	−0.494	−0.499	−0.502	−0.543
5247.956	(^{5}D)4d e^{6}G$_{3/2}$	(^{5}D)4f 1[3]$_{5/2}$	84938.220	103987.951		0.316	0.376	0.346	0.526	0.550
5251.225	(^{5}D)4d e^{6}G$_{5/2}$	(^{5}D)4f 1[4]$_{7/2}$	84844.819	103882.692		0.355	0.405	0.380	0.475	0.424
5253.649	(^{5}D)4d e^{6}G$_{11/2}$	(^{5}D)4f 3[5]$_{11/2}$	84296.833	103325.927	−0.191	−0.121	−0.121	−0.121	−0.104	−0.133
5257.119	(^{5}D)4d f^{4}D$_{7/2}$	(^{5}D)4f 2[5]$_{9/2}$	84685.198	103701.729		−0.028	−0.080	−0.054	−0.523	0.156
5260.254	(^{5}D)4d e^{6}G$_{13/2}$	(^{5}D)4f 4[7]$_{15/2}$	84035.121	103040.317	1.090	−−	−−	−−	1.065	−−
5264.180	(^{5}D)4d e^{6}G$_{7/2}$	(^{5}D)4f 2[5]$_{9/2}$	84710.703	103701.729		0.267	0.197	0.232	0.470	0.297
5265.985	(^{5}D)4d e^{6}G$_{13/2}$	(^{5}D)4f 4[7]$_{13/2}$	84035.121	103019.639		−0.760	−0.760	−0.760	−0.936	−0.871
5270.029	(^{5}D)4d e^{6}G$_{7/2}$	(^{5}D)4f 2[4]$_{9/2}$	84710.703	103680.640		−0.250	−0.310	−0.280	−0.097	−0.197

Table 4. cont.

λ(Å)	transition		χ_{low}(cm^{-1})	χ_{up}(cm^{-1})	loggf					
					exp	HR 6000	46 Aql	Aver	K09	RU98
5291.661	(^{5}D)4d e^{6}G$_{9/2}$	(^{5}D)4f 3[6]$_{11/2}$	84527.758	103420.158		0.460	0.510	0.485	0.561	0.544
5306.182	(^{5}D)4d f^{4}D$_{5/2}$	(^{5}D)4f 2[4]$_{7/2}$	84870.864	103711.562		−0.013	0.012	−0.001	0.049	0.044
5315.083	(^{5}D)4d f^{4}D$_{3/2}$	(^{5}D)4f 1[2]$_{5/2}$	85048.609	103857.755		−0.455	−0.455	−0.455	−0.422	−0.418
5316.214	(^{5}D)4d e^{6}G$_{13/2}$	(^{5}D)4f 4[6]$_{13/2}$	84035.121	102840.269	0.418	0.378	0.438	0.356	0.332	0.340
5318.055	(^{5}D)4d e^{6}G$_{9/2}$	(^{5}D)4f 3[4]$_{9/2}$	84527.758	103326.396		−0.136	−0.111	−0.123	−0.177	−0.226
5339.592	(^{5}D)4d e^{6}G$_{11/2}$	(^{5}D)4f 4[7]$_{13/2}$	84296.833	103019.639	0.568	0.438	0.518	0.478	0.516	0.517
5355.421	(^{5}D)4d f^{4}D$_{7/2}$	(^{5}D)4f 3[5]$_{9/2}$	84685.198	103352.673		−0.498	−0.478	−0.488	−0.203	−0.500
5358.872	(^{5}D)4d f^{4}D$_{7/2}$	(^{5}D)4f 3[4]$_{7/2}$	84685.198	103340.652		−0.426	−0.406	−0.416	−0.130	−0.609
5359.237	(^{5}D)4d e^{6}G$_{7/2}$	(^{5}D)4f 3[3]$_{5/2}$	84710.703	103364.847		−0.788	−0.808	−0.798	−1.112	−0.675
5366.210	(^{5}D)4d e^{6}G$_{7/2}$	(^{5}D)4f 3[4]$_{7/2}$	84710.703	103340.652		−0.265	−0.300	−0.282	−0.549	−0.196
5387.064	(^{5}D)4d e^{4}G$_{11/2}$	(^{5}D)4f 3[6]$_{13/2}$	84863.334	103421.165	0.593	0.479	0.534	0.506	0.500	0.499
5395.855	(^{5}D)4d ^{6}S$_{5/2}$	(^{5}D)4f 0[3]$_{7/2}$	85495.318	104022.912		0.328	0.398	0.363	0.415	0.285
5402.059	(^{5}D)4d e^{4}G$_{9/2}$	(^{5}D)4f 2[5]$_{11/2}$	85184.725	103691.045		0.469	0.502	0.485	0.472	0.469
5414.852	(^{5}D)4d e^{4}G$_{11/2}$	(^{5}D)4f 3[5]$_{11/2}$	84863.334	103325.927	−0.258	−0.274	−0.268	−0.271	−0.326	−0.324
5429.987	(^{5}D)4d e^{4}G$_{7/2}$	(^{5}D)4f 1[4]$_{9/2}$	85462.858	103873.991		0.350	0.400	0.375	0.429	0.427
5444.386	(^{5}D)4d ^{6}S$_{5/2}$	(^{5}D)4f 1[2]$_{5/2}$	85495.318	103857.755		−0.167	−0.157	−0.165	−0.153	−0.170
5451.316	(^{5}D)4d f^{4}D$_{7/2}$	(^{5}D)4f 4[2]$_{5/2}$	84685.198	103024.293		−0.753	−0.793	−0.773	−0.756	−0.649
5465.932	(^{5}D)4d e^{4}G$_{5/2}$	(^{5}D)4f 1[3]$_{7/2}$	85679.709	103969.766		0.331	0.406	0.368	0.515	0.348
5472.855	(^{5}D)4d f^{4}D$_{7/2}$	(^{5}D)4f 4[3]$_{5/2}$	84685.198	102952.122		−0.579	−0.579	−0.579	−0.723	−0.715
5475.826	(^{5}D)4d f^{4}D$_{7/2}$	(^{5}D)4f 4[3]$_{7/2}$	84685.198	102942.208		−0.225	−0.200	−0.212	−0.129	−0.080
5482.307	(^{5}D)4d e^{4}G$_{9/2}$	(^{5}D)4f 3[6]$_{11/2}$	85184.725	103420.158		0.363	0.455	0.409	0.393	0.413
5488.776	(^{5}D)4d e^{4}G$_{7/2}$	(^{5}D)4f 2[3]$_{7/2}$	85462.858	103676.798		−0.440	−0.420	−0.430	−0.468	−0.397
5492.398	(^{5}D)4d f^{4}D$_{7/2}$	(^{5}D)4f 4[4]$_{7/2}$	84685.198	102887.124		−0.039	−0.094	−0.066	−0.127	−0.097
5493.830	(^{5}D)4d f^{4}D$_{7/2}$	(^{5}D)4f 4[4]$_{9/2}$	84685.198	102882.375		0.143	0.228	0.185	0.252	0.259
5502.670	(^{5}D)4d e^{4}G$_{9/2}$	(^{5}D)4f 3[5]$_{9/2}$	85184.725	103352.673		−0.114	−0.094	−0.104	−0.179	−0.192
5506.199	(^{5}D)4d e^{4}G$_{11/2}$	(^{5}D)4f 4[7]$_{13/2}$	84863.334	103019.639	0.923	0.923	0.973	0.948	0.840	0.859
5510.783	(^{5}D)4d e^{4}G$_{9/2}$	(^{5}D)4f 3[5]$_{11/2}$	85184.725	103325.927	0.043	0.073	0.093	0.083	0.049	0.096
5529.053	(^{5}D)4d f^{4}D$_{5/2}$	(^{5}D)4f 3[2]$_{5/2}$	84870.864	102952.122		−0.146	−0.106	−0.126	−0.110	−0.258
5544.763	(^{5}D)4d e^{4}G$_{11/2}$	(^{5}D)4f 4[6]$_{11/2}$	84863.334	102893.377		0.149	0.129	0.139	0.130	0.139
5783.623	(^{5}D)4d e^{4}F$_{7/2}$	(^{5}D)4f 2[5]$_{9/2}$	86416.323	103701.729		0.241	0.266	0.253	0.267	0.365
5885.015	(^{5}D)4d e^{4}F$_{3/2}$	(^{5}D)4f 2[3]$_{5/2}$	86710.864	103698.466		0.158	0.188	0.173	0.336	0.298
5902.825	(^{5}D)4d e^{4}F$_{7/2}$	(^{5}D)4f 3[5]$_{9/2}$	86416.323	103352.673		0.346	0.416	0.381	0.415	0.416
5955.698	(^{5}D)4d e^{4}F$_{5/2}$	(^{5}D)4f 3[3]$_{7/2}$	86599.744	103385.735		0.155	0.205	0.180	0.234	0.252
5961.705	(^{5}D)4d e^{4}F$_{9/2}$	(^{5}D)4f 4[6]$_{11/2}$	86124.301	102893.377		0.593	0.742	0.667	0.685	0.675
5965.622	(^{5}D)4d e^{4}F$_{9/2}$	(^{5}D)4f 4[4]$_{9/2}$	86124.301	102882.375		0.016	0.096	0.056	0.091	0.068

Table 5. Lines due to (^{3}H)4d – (^{3}H)4f transitions of Fe II

Upper level		Lower level		λ(calc)	*log* gf					λ(obs),Notes
cm^{-1}		cm^{-1}		Å	HR6000	46 Aql	Aver	calc.		Å
122910.92	(^{3}H)4f 6[ ]$_{15/2}$	103617.58	(^{3}H)4d ^{4}H$_{13/2}$	5181.693	––	––	––	−3.314	K	
		103644.80	(^{3}H)4d ^{4}K$_{17/2}$	5189.014	––	––	––	−3.086	K	blend
		103706.53	(^{3}H)4d ^{4}K$_{15/2}$	5205.693	+0.075	+0.050	+0.063	−0.295	K	5205.714
		103832.05	(^{3}H)4d ^{4}K$_{13/2}$	5239.942	+0.225	+0.225	+0.225	+0.006	K	5239.948
		103878.37	(^{3}H)4d ^{4}I$_{15/2}$	5252.695	+0.070	+0.070	+0.070	−0.138	K	5252.702
		104064.67	(^{3}H)4d ^{4}I$_{13/2}$	5304.620	−0.314	−0.339	−0.327	−0.426	K	5304.60
		104119.71	(^{3}H)4d ^{2}K$_{15/2}$	5320.157	+0.078	+0.188	––	+0.133	K	5320.18
		104315.37	(^{3}H)4d ^{2}K$_{13/2}$	5376.136	+0.253	+0.253	+0.253	+0.112	K	5376.12
		104622.30	(^{3}H)4d ^{2}I$_{13/2}$	5466.362	+0.614	+0.614	+0.614	+0.713	K	5466.38
122952.73	(^{3}H)4f 6[9]$_{17/2}$	103644.80	(^{3}H)4d ^{4}K$_{17/2}$	5177.777	+0.513	+0.513	+0.513	−0.933	J	5177.77
		103706.53	(^{3}H)4d ^{4}K$_{15/2}$	5194.384	+0.724	+0.780	+0.752	+0.745	J	5194.387
		103878.37	(^{3}H)4d ^{4}I$_{15/2}$	5241.181	+0.655	+0.695	+0.675	+0.556	J	5241.183
		104119.71	(^{3}H)4d ^{2}K$_{15/2}$	5308.346	+0.500	+0.520	+0.510	+0.599	J	5308.35
122954.18	(^{3}H)4f 6[9]$_{19/2}$	103644.80	(^{3}H)4d ^{4}K$_{17/2}$	5177.388	+1.183	+1.253	+1.218	+1.166	J	5177.394
122990.62	(^{3}H)4f 6[]$_{13/2}$	103600.43	(^{3}H)4d ^{4}G$_{11/2}$	5155.811	––	––	––	−3.353	K	
		103617.58	(^{3}H)4d ^{4}H$_{13/2}$	5160.375	––	––	––	−1.722	K	
		103706.53	(^{3}H)4d ^{4}K$_{15/2}$	5184.178	––	––	––	−1.029	K	
		103751.66	(^{3}H)4d ^{4}H$_{11/2}$	5196.339	+0.114	+0.044	+0.079	−0.134	K	5196.345
		103832.05	(^{3}H)4d ^{4}K$_{13/2}$	5218.143	+0.100	+0.100	+0.100	−0.044	J	5218.149
		103878.37	(^{3}H)4d ^{4}I$_{15/2}$	5230.790	−1.200	−0.900	––	−1.233	K	very weak
		103973.78	(^{3}H)4d ^{4}K$_{11/2}$	5257.034	––	––	––	−0.894	K	
		104064.67	(^{3}H)4d ^{4}I$_{13/2}$	5282.281	−0.704	−0.604	−0.654	−1.118	K	
		104119.71	(^{3}H)4d ^{2}K$_{15/2}$	5297.687	−1.327	−1.327	−1.327	−0.953	K	very weak
		104174.27	(^{3}H)4d ^{4}I$_{11/2}$	5313.049	––	––	––	−0.987	K	
		104315.37	(^{3}H)4d ^{2}K$_{13/2}$	5353.192	+0.148	+0.068	+0.108	+0.205	K	blend, 5353.251
		104622.30	(^{3}H)4d ^{2}I$_{13/2}$	5442.643	+0.130	+0.075	+0.103	+0.070	J	5442.65
		104765.45	(^{3}H)4d ^{2}I$_{11/2}$	5485.393	−0.187	−0.187	−0.187	+0.150	K	5485.40
		106045.69	(^{3}H)4d ^{2}H$_{11/2}$	5899.835	+0.348	+0.348	+0.348	+0.250	K	5899.82
123002.28	(^{3}H)4f 6[ ]$_{11/2}$	103600.43	(^{3}H)4d ^{4}G$_{11/2}$	5152.712	+0.616	+0.616	+0.616	+0.639	K	5152.70
		103617.58	(^{3}H)4d ^{4}H$_{13/2}$	5157.271	––	––	––	+0.383	K	blend
		103751.66	(^{3}H)4d ^{4}H$_{11/2}$	5193.192	−0.767	−0.767:	−0.767	−0.444	K	weak
		103771.32	(^{3}H)4d ^{4}G$_{9/2}$	5198.501	≤−1.030	≤−1.230	––	−1.357	K	
		103832.05	(^{3}H)4d ^{4}K$_{13/2}$	5214.970	––	––	––	−2.624	K	
		103874.26	(^{3}H)4d ^{4}H$_{9/2}$	5226.478	––	––	––	−2.790	K	
		103973.78	(^{3}H)4d ^{4}K$_{11/2}$	5253.813	––	––	––	−4.096	K	
		104064.67	(^{3}H)4d ^{4}I$_{13/2}$	5279.028	––	––	––	−2.424	K	
		104174.27	(^{3}H)4d ^{4}I$_{11/2}$	5309.759	––	––	––	−2.421	K	
		104192.48	(^{3}H)4d ^{4}I$_{9/2}$	5314.899	––	––	––	−4.098	K	
		104315.37	(^{3}H)4d ^{2}K$_{13/2}$	5397.852	––	––	––	−3.473	K	
		104622.30	(^{3}H)4d ^{2}I$_{13/2}$	5439.191	––	––	––	−3.967	K	
		104765.45	(^{3}H)4d ^{2}I$_{11/2}$	5481.886	−1.264	−0.864	––	−1.294	K	very weak
		104807.21	(^{3}H)4d ^{2}G$_{9/2}$	5494.468	−0.923	−0.723	––	−1.632	K	very weak
		104916.55	(^{3}H)4d ^{4}F$_{9/2}$	5527.868	−1.031	−1.031	−1.031	−0.962	K	very weak
		105063.55	(^{3}F)4d ^{4}G$_{11/2}$	5572.983	−0.650	−0.550	−0.600	−0.753	K	
		105155.09	(^{3}F)4d ^{4}F$_{9/2}$	5601.568	––	––	––	−2.044	K	
		105288.85	(^{3}F)4d ^{4}H$_{13/2}$	5643.867	––	––	––	−1.416	K	
		105398.85	(^{3}F)4d ^{4}H$_{11/2}$	5679.136	––	––	––	−2.876	K	
		105524.46	(^{3}F)4d ^{4}H$_{9/2}$	5719.951	––	––	––	−4.454	K	
		105763.27	(^{3}F)4d ^{2}H$_{11/2}$	5799.189	––	––	––	−1.904	K	
		106018.64	(^{3}F)4d ^{2}H$_{9/2}$	5886.389	––	––	––	−6.492	K	
		106045.69	(^{3}H)4d ^{2}H$_{11/2}$	5895.778	––	––	––	−1.550	K	
		106097.52	(^{3}H)4d ^{2}H$_{9/2}$	5913.855	––	––	––	−2.902	K	
123007.91	(^{3}H)4f 6[8]$_{17/2}$	103644.80	(^{3}H)4d ^{4}K$_{17/2}$	5163.021	+0.571	+0.581	+0.576	+0.495	J	5163.00
		103706.53	(^{3}H)4d ^{4}K$_{15/2}$	5179.534	+0.640	+0.640	+0.640	+0.574	J	5179.54
		103878.37	(^{3}H)4d ^{4}I$_{15/2}$	5226.062	+0.829	+0.829	+0.829	+0.794	J	5226.07
		104119.71	(^{3}H)4d ^{2}K$_{15/2}$	5292.838	––	––	––	−1.288	K	

Table 5. cont.

Upper level		Lower level		λ(calc)	*log* gf					λ(obs),Notes
cm^{-1}		cm^{-1}		Å	HR6000	46 Aql	Aver	calc.		Å
123015.40	(^{3}H)4f 6[]$_{13/2}$	103600.43	(^{3}H)4d ^{4}G$_{11/2}$	5149.230	+ 0.485	+0.455	+0.470	+0.400	J	5149.25
		103617.58	(^{3}H)4d ^{4}H$_{13/2}$	5153.783	+ 0.684	+0.704	+0.694	+0.764	J	5153.78
		103706.53	(^{3}H)4d ^{4}K$_{15/2}$	5177.525	−−	−−	−−	−0.318	K	
		103751.66	(^{3}H)4d ^{4}H$_{11/2}$	5189.655	−−	−−	−−	−0.576	K	
		103832.05	(^{3}H)4d ^{4}K$_{11/2}$	5211.403	< −1.238	−−	−−	−2.671	K	
		103878.37	(^{3}H)4d ^{4}I$_{15/2}$	5224.017	−0.102	−0.102	−0.102	−0.146	J	5224.025
		103973.78	(^{3}H)4d ^{4}K$_{11/2}$	5250.193	−−	−−	−−	−3.971	K	
		104064.67	(^{3}H)4d ^{4}I$_{13/2}$	5275.373	−−	−−	−−	−1.672	K	
		104119.71	(^{3}H)4d ^{2}K$_{15/2}$	5290.740	−0.902	−0.902	−0.902	−1.303	K	5290.730
		104174.27	(^{3}H)4d ^{4}I$_{11/2}$	5306.061	−−	−−	−−	−2.648	K	
		104315.37	(^{3}H)4d ^{2}K$_{13/2}$	5346.098	−0.750	−0.750	−0.750	−1.957	K	
		104622.30	(^{3}H)4d ^{2}I$_{13/2}$	5435.311	−−	−−	−−	−2.414	K	
		104765.45	(^{3}H)4d ^{2}I$_{11/2}$	5477.945	−−	−−	−−	−1.272	K	
		106045.69	(^{3}H)4d ^{2}H$_{11/2}$	5891.220	−−	−−	−−	−1.347	K	
123018.43	(^{3}H)4f 6[]$_{15/2}$	103617.58	(^{3}H)4d ^{4}H$_{13/2}$	5152.978	+0.687	+0.697	+0.692	+0.763	J	5152.98
		103644.80	(^{3}H)4d ^{4}K$_{17/2}$	5160.218	−0.235	−0.235	−0.235	−0.357	K	5160.2
		103706.53	(^{3}H)4d ^{4}K$_{15/2}$	5176.713	+0.440	+0.440	+0.440	+0.385	J	5176.72
		103832.05	(^{3}H)4d ^{4}K$_{13/2}$	5210.580	−−	−−	−−	−1.050	K	
		103878.37	(^{3}H)4d ^{4}I$_{15/2}$	5223.190	+0.487	+0.487	+0.487	+0.427	K	blend
		104064.67	(^{3}H)4d ^{4}I$_{13/2}$	5274.530	−1.193	−1.043	−−	−1.138	K	very weak
		104119.71	(^{3}H)4d ^{2}K$_{15/2}$	5289.892	−0.656	−0.656	−0.656	−0.923	K	5289.899
		104315.37	(^{3}H)4d ^{2}K$_{13/2}$	5345.232	−−	−−	−−	−2.411	K	
		104622.30	(^{3}H)4d ^{2}I$_{13/2}$	5434.415	−−	−−	−−	−1.487	K	
123026.35	(^{3}H)4f 6[]$_{9/2}$	103600.43	(^{3}H)4d ^{4}G$_{11/2}$	5146.326	−−	−−	−−	−4.447	K	
		103751.66	(^{3}H)4d ^{4}H$_{11/2}$	5186.706	−0.120	−0.184	−0.152	−0.149	J	5186.722
		103771.32	(^{3}H)4d ^{4}G$_{9/2}$	5192.002	+0.080	+0.080	+0.080	+0.066	J	5192.010
		103814.55	(^{3}H)4d ^{4}G$_{7/2}$	5203.685	−−	−−	−−	−2.154	K	
		103874.26	(^{3}H)4d ^{4}H$_{9/2}$	5219.909	−0.455:	−0.455:	−0.455	−0.440	K	blend
		103973.78	(^{3}H)4d ^{4}K$_{11/2}$	5247.175	−−	−−	−−	−3.791	K	
		103986.33	(^{3}H)4d ^{4}G$_{7/2}$	5250.632	−0.300	−0.300 ?	−0.300	−2.907	K	5250.609
		104174.27	(^{3}H)4d ^{4}I$_{11/2}$	5302.979	−−	−−	−−	−2.785	K	
		104192.48	(^{3}H)4d ^{4}I$_{9/2}$	5308.106	−−	−−	−−	−2.122	K	
		104481.59	(^{3}H)4d ^{2}F$_{7/2}$	5390.860	−−	−−	−−	−1.070	K	
		104765.45	(^{3}H)4d ^{4}I$_{11/2}$	5474.660	−−	−−	−−	−1.961	K	
		104807.21	(^{3}H)4d ^{2}G$_{9/2}$	5487.209	+0.334	+0.334	+0.334	+0.348	J	5497.21
		104916.55	(^{3}H)4d ^{4}F$_{9/2}$	5520.339	−1.500	≤−1.50	−−	−1.382	K	
		105123.00	(^{3}H)4d ^{2}G$_{7/2}$	5583.996	−−	−−	−−	−3.472	K	
		105220.60	(^{3}H)4d ^{4}F$_{9/2}$	5614.605	−−	−−	−−	−1.910	K	
		106045.69	(^{3}H)4d ^{2}H$_{11/2}$	5887.421	−0.260	−0.172	−0.216	−0.132	K	5887.42
		106097.52	(^{3}H)4d ^{2}H$_{9/2}$	5905.446	−−	−−	−−	−0.710	K	
123037.43	(^{3}H)4f 6[]$_{11/2}$	103600.43	(^{3}H)4d ^{4}G$_{11/2}$	5143.394	−−	−−	−−	−1.365	K	
		103617.58	(^{3}H)4d ^{4}H$_{13/2}$	5147.936	−−	−−	−−	−2.244	K	
		103751.66	(^{3}H)4d ^{4}H$_{11/2}$	5183.727	+0.303	+0.303	+0.303	+0.240	K	5183.713
		103771.32	(^{3}H)4d ^{4}G$_{9/2}$	5189.016	−0.070	−0.070	−0.070	−0.190	K	5189.013
		103832.05	(^{3}H)4d ^{4}K$_{13/2}$	5205.425	−0.394	−0.594	−−	−0.552	K	5205.427
		103874.26	(^{3}H)4d ^{4}H$_{9/2}$	5216.891	−−	−−	−−	−0.463	K	
		103973.78	(^{3}H)4d ^{4}K$_{11/2}$	5244.125	−−	−−	−−	−1.886	K	
		104064.67	(^{3}H)4d ^{4}I$_{13/2}$	5269.248	−0.698	noise	−−	−0.828	K	5269.235
		104174.27	(^{3}H)4d ^{4}I$_{11/2}$	5299.864	−−	−−	−−	−1.744	K	
		104192.48	(^{3}H)4d ^{4}I$_{9/2}$	5304.985	−−	−−	−−	−2.176	K	
		104315.37	(^{3}H)4d ^{2}K$_{13/2}$	5339.807	−0.633	−0.533	−0.583	−0.768	K	very weak
		104622.30	(^{3}H)4d ^{2}I$_{13/2}$	5428.808	−0.479	−0.379	−0.429	−0.387	K	5288.8
		104765.45	(^{3}H)4d ^{2}I$_{11/2}$	5471.340	−0.994	−−	−−	−0.906	K	very weak
		104807.21	(^{3}H)4d ^{2}G$_{9/2}$	5483.874	+0.096	+0.171	+0.134	+0.120	K	5483.85
		104916.55	(^{3}H)4d ^{4}F$_{9/2}$	5516.963	≤−2.00	≤−2.00	−−	−1.760	K	not obs
		106045.69	(^{3}H)4d ^{2}H$_{11/2}$	5883.582	+0.223	+0.383	−−	+0.259	K	5883.58
		106097.52	(^{3}H)4d ^{2}H$_{9/2}$	5901.584	−−	−−	−−	−0.574	K	

Table 5. cont.

Upper level		Lower level		λ(calc)	*log* gf					λ(obs),Notes
cm^{-1}		cm^{-1}		Å	HR 6000	46 Aql	Aver	calc.		Å
123168.68	(^{3}H)4f 5[]$_{13/2}$	103600.43	(^{3}H)4d ^{4}G$_{11/2}$	5108.895	−1.234	−1.234	−1.234	−0.921	K	weak,noise
		103617.58	(^{3}H)4d ^{4}H$_{13/2}$	5113.377	−−	−−	−−	−2.499	K	
		103706.53	(^{3}H)4d ^{4}K$_{15/2}$	5136.747	−−	−−	−−	−1.281	K	blend
		103751.66	(^{3}H)4d ^{4}H$_{11/2}$	5148.687	−0.033	−0.083	−0.058	+0.020	K	5148.7
		103832.05	(^{3}H)4d ^{4}K$_{11/2}$	5170.092	−−	−−	−−	−1.042	K	5170.1,blend
		103878.37	(^{3}H)4d ^{4}I$_{15/2}$	5182.507	−−	−−	−−	−1.516	K	
		103973.78	(^{3}H)4d ^{4}K$_{11/2}$	5208.267	+0.136	+0.136	+0.136	−0.286	K	5208.268
		104064.67	(^{3}H)4d ^{4}I$_{13/2}$	5233.046	+0.215	+0.215	+0.215	+0.122	K	5233.041
		104119.71	(^{3}H)4d ^{2}K$_{15/2}$	5248.167	−−	−−	−−	−2.450	K	
		104174.27	(^{3}H)4d ^{4}I$_{11/2}$	5263.242	−0.320	−0.320	−0.320	−0.689	K	
		104315.37	(^{3}H)4d ^{2}K$_{13/2}$	5302.633	−−	−−	−−	−0.553	K	blend
		104622.30	(^{3}H)4d ^{2}I$_{13/2}$	5390.389	−0.405	−0.405	−0.405	+0.021	K	5390.38
		104765.45	(^{3}H)4d ^{2}I$_{11/2}$	5432.319	+0.530	+0.530	+0.530	+0.489	K	5432.31
		106045.69	(^{3}H)4d ^{2}H$_{11/2}$	5838.483	−0.547	−0.547	−0.547	−0.332	K	weak,noise
123193.09	(^{3}H)4f 5[]$_{15/2}$	103617.58	(^{3}H)4d ^{4}H$_{13/2}$	5107.001	−0.985	−1.085	−1.035	−1.475	K	very weak
		103644.80	(^{3}H)4d ^{4}K$_{17/2}$	5114.112	−−	−−	−−	−2.416	K	
		103706.53	(^{3}H)4d ^{4}K$_{15/2}$	5130.313	−0.300	−0.450	−−	−0.493	K	5130.3
		103832.05	(^{3}H)4d ^{4}K$_{13/2}$	5163.574	+0.779	+0.850	+0.815	+0.896	J	5163.5
		103878.37	(^{3}H)4d ^{4}I$_{15/2}$	5175.957	−0.429	−0.630	−−	−0.465	K	5175.95
		104064.67	(^{3}H)4d ^{4}I$_{13/2}$	5226.368	+0.397	+0.360	+0.379	−0.211	J	5226.367
		104119.71	(^{3}H)4d ^{2}K$_{15/2}$	5241.450	−0.100	−0.150	−0.125	−0.359	J	5241.465
		104315.37	(^{3}H)4d ^{2}K$_{13/2}$	5295.776	−0.538	≤−0.588	−−	−0.334	K	5295.773
		104622.30	(^{3}H)4d ^{2}I$_{13/2}$	5383.304	+0.401	+0.370	+0.386	+0.157	K	5383.32
123219.199	(^{3}H)4f 5[8]$_{17/2}$	103644.80	(^{3}H)4d ^{4}K$_{17/2}$	5107.290	−−	−−	−−	−0.997	K	weak,blend
		103706.53	(^{3}H)4d ^{4}K$_{15/2}$	5123.448	+0.322	+0.332	+0.330	+0.390	K	5123.45
		103878.37	(^{3}H)4d ^{4}I$_{15/2}$	5168.969	−−	−−	−−	+0.201	K	blend
		104119.71	(^{3}H)4d ^{4}K$_{15/2}$	5234.285	+0.967	1.067	+1.017	+0.959	K	5234.283
123238.44	(^{3}H)4f 5[]$_{15/2}$	103617.58	(^{3}H)4d ^{4}H$_{13/2}$	5095.196	−0.728	−0.878	−−	−0.884	K	very weak,blend
		103644.80	(^{3}H)4d ^{4}K$_{17/2}$	5102.275	−−	−−	−−	−2.988	K	
		103706.53	(^{3}H)4d ^{4}K$_{15/2}$	5118.401	−0.270	−0.270	−0.270	−0.239	J	5118.404
		103832.05	(^{3}H)4d ^{4}K$_{13/2}$	5151.507	−0.059	−0.059:	−0.059	−0.608	K	5151.52,blend
		103878.37	(^{3}H)4d ^{4}I$_{15/2}$	5163.831	−0.626	−0.626	−0.626	−0.495	K	5163.82
		104064.67	(^{3}H)4d ^{4}I$_{13/2}$	5214.007	+0.650	+0.795	−−	+0.868	K	5214.96,blend
		104119.71	(^{3}H)4d ^{2}K$_{15/2}$	5229.017	+0.065	+0.015	+0.040	−0.096	J	5229.038
		104315.37	(^{3}H)4d ^{2}K$_{13/2}$	5283.085	+0.343	+0.313	+0.328	+0.323	J	5283.093
		104622.30	(^{3}H)4d ^{2}I$_{13/2}$	5370.189	−−	−−	−−	−1.820	K	
123249.65	(^{3}H)4f 5[]$_{13/2}$	103600.43	(^{3}H)4d ^{4}G$_{11/2}$	5087.842	−0.496	−0.496	−0.496	−0.402	J	5087.85
		103617.58	(^{3}H)4d ^{4}H$_{13/2}$	5092.287	−2.477	−−	−−	−3.143	K	very weak
		103706.53	(^{3}H)4d ^{4}K$_{15/2}$	5115.465	−0.950	−1.015	−0.983	−1.004	K	5115.5
		103751.66	(^{3}H)4d ^{4}H$_{11/2}$	5127.305	+0.450:	+0.450	+0.450	+0.360	J	5127.32, blend
		103832.05	(^{3}H)4d ^{4}K$_{13/2}$	5148.533	+0.300	+0.353	+0.326	+0.361	J	5148.52
		103878.37	(^{3}H)4d ^{4}I$_{15/2}$	5160.844	−−	−−	−−	−1.782	K	
		103973.78	(^{3}H)4d ^{4}K$_{11/2}$	5186.389	+0.060	+0.100	+0.080	+0.226	J	5186.396
		104064.67	(^{3}H)4d ^{4}I$_{13/2}$	5210.960	−0.280	−0.320	−0.300	−0.425	K	5210.964
		104119.71	(^{3}H)4d ^{2}K$_{15/2}$	5225.953	−−	−−	−−	−0.776	K	
		104174.27	(^{3}H)4d ^{4}I$_{11/2}$	5240.901	−0.550	−0.500	−0.525	−0.474	K	5240.911
		104315.37	(^{3}H)4d ^{2}K$_{13/2}$	5279.957	−0.350	−0.400	−0.375	−0.737	K	blend
		104622.30	(^{3}H)4d ^{2}I$_{13/2}$	5366.958	+0.143	+0.093	+0.118	+0.040	J	5366.95
		104765.45	(^{3}H)4d ^{2}I$_{11/2}$	5408.522	−−	−−	−−	−2.264	K	
		106045.69	(^{3}H)4d ^{2}H$_{11/2}$	5811.004	+0.050	bad sp.	−−	−0.189	K	5811.00

Table 5. cont.

Upper level		Lower level		λ(calc)	*log* gf				λ(obs),Notes	
cm^{-1}		cm^{-1}		Å	HR 6000	46 Aql	Aver	calc.		Å
123251.47	(^{3}H)4f 5[]$_{11/2}$	103600.43	(^{3}H)4d ^{4}G$_{11/2}$	5087.371	−−	−−	−−	−1.402	K	
		103617.58	(^{3}H)4d ^{4}H$_{13/2}$	5091.815	−−	−1.000	−−	−2.881	K	blend
		103751.66	(^{3}H)4d ^{4}H$_{11/2}$	5126.827	+0.185	+0.085	+0.135	−0.224	J	5126.84, bl
		103771.32	(^{3}H)4d ^{4}G$_{9/2}$	5132.001	+0.180	+0.150	+0.165	+0.097	J	5132.0
		103832.05	(^{3}H)4d ^{4}K$_{13/2}$	5148.050	−−	−−	−−	−2.123	K	very weak
		103874.26	(^{3}H)4d ^{4}H$_{9/2}$	5159.265	+0.140	+0.140	+0.140	+0.005	J	5159.29
		103973.78	(^{3}H)4d ^{4}K$_{11/2}$	5185.899	+0.080	+0.080	+0.080	+0.065	J	5185.901
		104064.67	(^{3}H)4d ^{4}I$_{13/2}$	5210.466	−−	−−	−−	−0.582	K	5210.546,blend
		104174.27	(^{3}H)4d ^{4}I$_{11/2}$	5240.401	−0.100	−0.200	−0.150	−0.207	J	5240.405
		104192.48	(^{3}H)4d ^{4}I$_{9/2}$	5245.408	−−	−−	−−	−1.056	K	
		104315.37	(^{3}H)4d ^{2}K$_{13/2}$	5279.449	−0.850	−0.850	−0.850	−1.299	K	weak
		104622.30	(^{3}H)4d ^{2}I$_{13/2}$	5366.433	−1.000	−1.250	−−	−3.032	K	very weak
		104765.45	(^{3}H)4d ^{2}I$_{11/2}$	5407.990	+0.040	+0.040	+0.040	+0.035	J	5407.99
		104807.21	(^{3}H)4d ^{2}G$_{9/2}$	5420.234	−0.750	−0.750	−0.750	−2.508	K	blend
		104916.55	(^{3}H)4d ^{4}F$_{9/2}$	5452.558	−0.500	−0.500	−0.500	−0.785	K	5452.55
		106045.69	(^{3}H)4d ^{2}H$_{11/2}$	5810.389	bad sp.	−0.500	−−	−1.336	K	blend
		106097.52	(^{3}H)4d ^{2}H$_{9/2}$	5827.945	+0.190	+0.190	+0.190	+0.037	K	5827.95
123258.99	(^{3}H)4f 5[]$_{9/2}$	103600.43	(^{3}H)4d ^{4}G$_{11/2}$	5085.425	−1.369	−−	−−	−1.127	K	weak,noise
		103751.66	(^{3}H)4d ^{4}H$_{11/2}$	5124.850	+0.043	+0.043	+0.043	+0.037	K	5124.82
		103771.32	(^{3}H)4d ^{4}G$_{9/2}$	5130.020	+0.287	+0.287	+0.287	+0.257	K	5130.0
		103814.55	(^{3}H)4d ^{4}G$_{7/2}$	5141.426	−−	−−	−−	−3.748	K	
		103874.26	(^{3}H)4d ^{4}H$_{9/2}$	5157.263	−−	−−	−−	−0.606	K	blend
		103973.78	(^{3}H)4d ^{4}K$_{11/2}$	5183.877	−−	−−	−−	−2.156	K	
		103986.33	(^{3}H)4d ^{4}H$_{7/2}$	5187.253	−−	−−	−−	−4.544	K	
		104174.27	(^{3}H)4d ^{4}I$_{11/2}$	5238.336	−−	−−	−−	−4.551	K	
		104192.48	(^{3}H)4d ^{4}I$_{9/2}$	5243.339	−−	−−	−−	−3.145	K	
		104481.59	(^{3}H)4d ^{2}F$_{7/2}$	5324.070	−0.548	−0.648	−0.598	−0.588	K	weak,blend
		104765.45	(^{3}H)4d ^{2}I$_{11/2}$	5405.791	−−	−−	−−	−2.078	K	
		104807.21	(^{3}H)4d ^{2}G$_{9/2}$	5418.025	+0.001	−0.241	−−	−0.061	K	blend
		104916.55	(^{3}H)4d ^{4}F$_{9/2}$	5450.323	−0.471	−0.521	−0.496	−0.373	K	
		105123.00	(^{3}H)4d ^{2}G$_{7/2}$	5512.367	−0.917	<−0.917	−−	−1.134	K	
		105220.60	(^{3}H)4d ^{4}F$_{7/2}$	5542.193	−−	−−	−−	−1.725	K	
		106045.69	(^{3}H)4d ^{2}H$_{11/2}$	5807.851	−0.226	−0.126	−0.176	−0.455	K	
		106097.52	(^{3}H)4d ^{2}H$_{9/2}$	5825.392	−−	−−	−−	−0.790	K	
123270.34	(^{3}H)4f 5[]$_{11/2}$	103600.43	(^{3}H)4d ^{4}G$_{11/2}$	5082.492	−1.101	−0.801	−−	−0.654	K	blend
		103617.58	(^{3}H)4d ^{4}H$_{13/2}$	5086.927	−−	−−	−−	−2.184	K	
		103751.66	(^{3}H)4d ^{4}H$_{11/2}$	5121.871	+0.375	+0.375	+0.375	+0.348	K	5121.89
		103771.32	(^{3}H)4d ^{4}G$_{9/2}$	5127.035	−0.458	−0.478	−0.468	−0.587	K	
		103832.05	(^{3}H)4d ^{4}K$_{11/2}$	5143.054	−0.459	−0.459	−0.459	−0.450	K	
		103874.26	(^{3}H)4d ^{4}H$_{9/2}$	5154.246	+0.133	+0.133	+0.133	+0.130	K	5154.25
		103973.78	(^{3}H)4d ^{4}K$_{11/2}$	5180.829	−0.217	−0.217	−0.217	−0.491	K	
		104064.67	(^{3}H)4d ^{4}I$_{13/2}$	5205.347	−1.188	−0.888	−−	−0.854	K	
		104174.27	(^{3}H)4d ^{4}I$_{11/2}$	5235.223	−0.372	−0.372	−0.372	−0.537	K	5235.225
		104192.48	(^{3}H)4d ^{4}I$_{9/2}$	5240.220	−−	−−	−−	−1.237	K	
		104315.37	(^{3}H)4d ^{2}K$_{13/2}$	5274.195	−−	−−	−−	−1.382	K	
		104622.30	(^{3}H)4d ^{2}I$_{13/2}$	5361.004	−0.438	−0.288	−−	−0.419	K	
		104765.45	(^{3}H)4d ^{2}I$_{11/2}$	5402.476	−−	−−	−−	−1.619	K	
		104807.21	(^{3}H)4d ^{2}G$_{9/2}$	5414.696	−0.192	−0.152	−0.172	−0.156	K	blend
		104916.55	(^{3}H)4d ^{4}F$_{9/2}$	5446.953	−0.709	−0.909	−−	−0.733	K	
		106045.69	(^{3}H)4d ^{2}H$_{11/2}$	5804.025	+0.022	−0.028	−0.003	−0.041	K	5804.02
		106097.52	(^{3}H)4d ^{2}H$_{9/2}$	5821.543	−−	−−	−−	−3.123	K	
123355.49	(^{3}H)4f 4[]$_{13/2}$	103600.43	(^{3}H)4d ^{4}G$_{11/2}$	5060.583	−−	−−	−−	−1.129	K	
		103617.58	(^{3}H)4d ^{4}H$_{13/2}$	5064.980	−−	−−	−−	−3.032	K	
		103706.53	(^{3}H)4d ^{4}K$_{15/2}$	5087.910	−−	−−	−−	−1.855	K	
		103751.66	(^{3}H)4d ^{4}H$_{11/2}$	5099.623	−0.281	−0.481	−0.381	−0.218	K	5099.6

Table 5. cont.

Upper level		Lower level		λ(calc)	*log* gf					λ(obs),Notes
cm^{-1}		cm^{-1}		Å	HR 6000	46 Aql	Aver	calc.		Å
		103832.05	(^{3}H)4d ^{4}K$_{13/2}$	5120.621	−0.650	−0.800	−0.725	−1.186	K	5120.62
		103878.37	(^{3}H)4d ^{4}I$_{15/2}$	5132.799	−−	−−	−−	−3.301	K	
		103973.78	(^{3}H)4d ^{4}K$_{11/2}$	5158.067	+0.715	+0.715	+0.715	+0.781	K	5158.05
		104064.67	(^{3}H)4d ^{4}I$_{13/2}$	5182.370	−0.081	−0.051	−0.066	+0.049	K	5182.37
		104119.71	(^{3}H)4d ^{2}K$_{15/2}$	5197.198	−−	−−	−−	−1.494	K	
		104174.27	(^{3}H)4d ^{4}I$_{11/2}$	5211.982	−−	−−	−−	−1.774	K	
		104315.37	(^{3}H)4d ^{2}K$_{13/2}$	5250.606	−0.298	−0.298	−0.298	−0.774	K	5250.609
		104622.30	(^{3}H)4d ^{2}I$_{13/2}$	5336.635	−0.276	−0.226	−0.251	−0.241	K	5336.62
		104765.45	(^{3}H)4d ^{2}I$_{11/2}$	5377.729	+0.176	+0.126	+0.151	−0.165	K	5377.71
		106045.69	(^{3}H)4d ^{2}H$_{11/2}$	5775.473	−−	−−	−−	−0.703	K	no spect.
123396.25	(^{3}H)4f 4[]$_{15/2}$	103617.58	(^{3}H)4d ^{4}H$_{13/2}$	5054.542	−−	−−	−−	−2.432	K	
		103644.80	(^{3}H)4d ^{4}K$_{17/2}$	5061.508	−−	−−	−−	−5.014	K	
		103706.53	(^{3}H)4d ^{4}K$_{15/2}$	5077.377	−−	−−	−−	−1.424	K	
		103832.05	(^{3}H)4d ^{4}K$_{13/2}$	5109.953	−0.197	−0.197	−0.197	−0.064	K	5109.29
		103878.37	(^{3}H)4d ^{4}I$_{15/2}$	5122.080	−−	−−	−−	−1.735	K	
		104064.67	(^{3}H)4d ^{4}I$_{13/2}$	5171.443	+0.230	+0.230	+0.230	+0.289	K	5171.45
		104119.71	(^{3}H)4d ^{2}K$_{15/2}$	5186.209	−−	−−	−−	−2.259	K	
		104315.37	(^{3}H)4d ^{2}K$_{13/2}$	5239.390	+0.800	+0.850	+0.825	+0.860	K	5239.394
		104622.30	(^{3}H)4d ^{2}I$_{13/2}$	5325.048	+0.322	+0.302	+0.312	+0.201	K	
123441.10	(^{3}H)4f 4[]$_{11/2}$	103600.43	(^{3}H)4d ^{4}G$_{11/2}$	5038.747	−−	−−	−−	−3.261	K	
		103617.58	(^{3}H)4d ^{4}H$_{13/2}$	5043.107	−−	−−	−−	−4.974	K	
		103751.66	(^{3}H)4d ^{4}H$_{11/2}$	5077.449	−−	−−	−−	−2.014	K	
		103771.32	(^{3}H)4d ^{4}G$_{9/2}$	5082.524	−0.776	−0.776	−0.776	−0.363	K	blend
		103832.05	(^{3}H)4d ^{4}K$_{13/2}$	5098.265	−−	−−	−−	−1.713	K	
		103874.26	(^{3}H)4d ^{4}H$_{9/2}$	5109.263	−0.501	−0.201	−0.351	+0.054	K	
		103973.78	(^{3}H)4d ^{4}K$_{11/2}$	5135.383	−0.428	−0.463	−0.445	−1.305	K	
		104064.67	(^{3}H)4d ^{4}I$_{13/2}$	5159.472	−−	−−	−−	−2.203	K	
		104174.27	(^{3}H)4d ^{4}I$_{11/2}$	5188.822	+0.184	+0.184	+0.184	+0.228	K	5188.831
		104192.48	(^{3}H)4d ^{4}I$_{9/2}$	5193.731	+0.675	+0.725	+0.700	+0.533	K	5193.74
		104315.37	(^{3}H)4d ^{2}K$_{13/2}$	5227.103	−−	−−	−−	−1.337	K	
		104622.30	(^{3}H)4d ^{2}I$_{13/2}$	5312.357	−−	−−	−−	−1.799	K	
		104765.45	(^{3}H)4d ^{2}I$_{11/2}$	5353.077	−−	−−	−−	−0.252	K	blend
		104807.21	(^{3}H)4d ^{2}G$_{9/2}$	5365.074	−−	−−	−−	−1.303	K	
		104916.55	(^{3}H)4d ^{4}F$_{9/2}$	5396.741	−−	−−	−−	−3.494	K	
		106045.69	(^{3}H)4d ^{2}H$_{11/2}$	5747.049	−−	−−	−−	−1.647	K	
		106097.52	(^{3}H)4d ^{2}H$_{9/2}$	5764.224	−−	−−	−−	−0.340	K	

Table 6. More new Fe II identified lines

λ(obs)	λ(calc)		Lower level		Upper level		log gf	
Å	Å			cm^{-1}		cm^{-1}	stellar	calc.
4042.72	4042.741	K	(^{4}P)4s4p(^{3}P) ^{6}P$_{5/2}$	89444.458	(^{5}D)6d ^{6}D$_{7/2}$	114173.163	−1.035	−1.243
4123.65	4123.667	K	(^{5}D)5p ^{6}D$_{9/2}$	88723.400	(^{5}D)6d ^{6}P$_{7/2}$	112966.820	−1.453	−1.996
4145.98	4145.922	K	(^{5}D)5p ^{6}D$_{7/2}$	88853.533	(^{5}D)6d ^{6}P$_{7/2}$	112966.820	−1.741	−1.847
4187.72	4187.733	K	(^{5}D)5p ^{6}F$_{7/2}$	90300.625	(^{5}D)6d ^{6}D$_{7/2}$	114173.163	−1.177	−1.505
−−	4192.154	K	(^{5}D)5p ^{6}D$_{5/2}$	89119.457	(^{5}D)6d ^{6}P$_{7/2}$	112966.820	−1.882	−2.153
5039.704	5039.700	J	b(^{3}F)4p ^{4}D$_{7/2}$	93129.900	(^{5}D)6d ^{6}P$_{7/2}$	112966.820	−0.559	−5.578
5129.929	5129.915	J	(^{4}D)4s4p ^{6}P$_{5/2}$	94685.090	(^{5}D)6d ^{6}D$_{7/2}$	114173.163	−0.285	−4.251
5131.450	5131.445	J	b(^{3}F)4p u^{4}F$_{9/2}$	93484.580	(^{5}D)6d ^{6}P$_{7/2}$	112966.820	−1.112	−7.130
5134.070	5134.014	K	(^{3}P)4p ^{2}D$_{5/2}$	94700.660	(^{5}D)6d ^{6}D$_{7/2}$	114173.163	−0.225	−5.483